ATLAS CSC NOTE 10
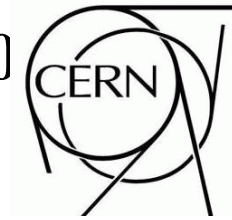
Sensitivity to an invisibly decaying Higgs boson with ATLAS data

P. Gagnon, R. Goncalo, G. Hanninger, A. Ludwig, W. Mader, G. Oakham, M. Schram, S. Subramania

Abstract

Many extensions of the Standard Model include Higgs bosons decaying predominantly or partially to non-interacting particles such as the SUSY Lightest Supersymmetric Particle (LSP). To set limits on the production cross-section times the branching fraction to invisible decay products of such Higgs bosons with the ATLAS detector requires an examination of specific production modes such as the associated production (ZH) or the vector boson fusion (VBF) process. The predominant Standard Model backgrounds for these processes are $ZZ \to \ell\ell\nu\nu$ for the ZH channel and jets from QCD processes and $W^{\pm}$ or Z bosons produced in association with jets for the VBF channel. The sensitivity to an invisibly decaying Higgs boson is investigated in this paper using fully simulated ATLAS data for both signal and background. The ATLAS potential for triggering these events is also discussed.

1   Introduction

Some extensions of the Standard Model predict that Higgs bosons could decay into stable neutral weakly interacting particles, leading to invisible Higgs boson decays. The Higgs boson decay products could be for example neutralinos, gravitinos, gravitons or Majorons [1-3]. In the case of the Minimal Supersymmetric Standard Model (MSSM), if R-parity is conserved, Higgs bosons decaying into a pair of neutralinos may in some cases even dominate [1]. Being the lightest supersymmetric particles, neutralinos would be stable and would leave the detector without decaying, remaining invisible. If R-parity is violated, then Higgs bosons could decay into Majorons, which would interact too weakly to allow detection [2]. Some theories with extra dimensions also predict invisible Higgs boson decays, and have the added advantage of generating neutrino masses [3]. This search is sensitive to any boson coupling to Z or W and decaying invisibly. The combined LEP Higgs boson mass limit in this channel is 114.4 GeV [4].

At the Large Hadron Collider, Higgs boson production could occur through several mechanisms. To select and identify events with an invisibly decaying Higgs boson one must be able to trigger on a signature that is visible in the event. This is possible for channels such as Vector Boson Fusion (VBF) qqH [5], $t\bar{t}H$ [6] and the associated production processes, ZH and $W^{\pm}H$ [7, 8]. Although gluon fusion has a much higher Higgs boson production cross-section than these modes [9], it is not possible to trigger on these events when the Higgs boson decays invisibly.

In this paper, the ATLAS sensitivity to an invisibly decaying Higgs boson is determined in a way that does not depend on a specific extension of the Standard Model. The analysis uses the variable ξ^2 which is defined as,

$$\xi^2 = BR(H \to inv.)\frac{\sigma_{BSM}}{\sigma_{SM}} \tag{1}$$

where σ_{BSM} represents the "Beyond the Standard Model" cross-section and σ_{SM} represents the Standard Model cross-section. In the case for which the Higgs boson decays entirely to the invisible mode, ξ^2 is the ratio between the non-Standard Model cross-section and the Standard Model cross-section. Only two of the three possible production modes are considered in this paper, VBF and associated production. In addition, for associated production, only the ZH mode is considered as the background to the $W^{\pm}H$ signal is overwhelming [10].

In this paper, the Monte Carlo samples, for both the VBF and the ZH channels, the trigger, the event selection, the systematic uncertainties and the results are discussed. We conclude by summarizing the limits on ξ^2 for an invisibly decaying Higgs boson.

This analysis compares signals and backgrounds that have been generated using Standard Model processes. The Higgs boson signal events are simulated to be invisible by changing the properties of the Higgs boson decay chain. In reality an invisibly decaying Higgs boson would be expected to result from a process not contained within the Standard Model, and in this case backgrounds associated with this new physics would be important. However, consideration of "Beyond the Standard Model" backgrounds is beyond the scope of this paper as they would have to be considered in the context of each specific model. This analysis assumes Standard Model backgrounds and serves as a limiting case for the indication of a particle that behaves like a Higgs boson that is not consistent with the Standard Model.

2   The Vector Boson Fusion qqH production channel

The vector boson fusion (VBF) channel has the second largest production mode after gluon fusion and has the largest production cross-section for observable invisible Higgs boson decays. The VBF invisible Higgs boson production mode, Figure 1, is characterized by two outgoing jets resulting from the interacting quarks, and large missing transverse energy from the Higgs boson. The topology of the jets is

particularly useful in selecting the events as the jets are preferentially separated in pseudo-rapidity (η) and are correlated in the azimuthal angle ϕ. In addition, the lack of colour flow between the two jets leads to minimal jet activity between the two tagging jets which is potentially useful for selecting events. At high luminosity however, central jet activity resulting from overlapping events may become problematic for cuts based on this event characteristic.
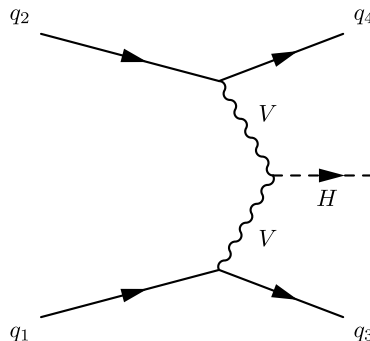

Figure 1: Feynman diagram of the VBF process. The V represents either a Z or W boson.

The study of the VBF channel for this paper includes a mass scan with an estimate of the sensitivity to Higgs boson masses between 110 to 250 GeV. This is based on fully reconstructed signal and background events. In addition to the sensitivity, the trigger acceptance for this channel has been investigated.

2.1 Monte Carlo generation for the VBF analysis

Signal and background samples were generated using the standard version of ATLAS software used for this set of papers. The samples were used to determine the sensitivity of ATLAS to an invisible Higgs boson, taking into account the trigger and analysis efficiencies. A number of backgrounds with signatures similar to the signal have been studied and are listed here. In all cases, ℓ represents e or μ.

1. Dijet production from QCD processes form a major background due to the very large cross-section for these processes. Fake missing energy measurements can arise from poorly instrumented regions or inefficiencies in the detector.

2. W+jet processes with $W \rightarrow \ell\nu$ mimic the signal when the lepton is outside the detector acceptance. The neutrino provides the missing energy signature.

3. Z+jet processes with $Z \rightarrow \nu\nu$ constitute an irreducible background.

4. Z+jet with $Z \rightarrow \ell\ell$ forms a background to the signal when the leptons are not within the acceptance of the detector.

Event generation for the VBF channel has proved challenging given that the predicted η distributions of tagging jets differ greatly according to the event simulation model used. The HERWIG-JIMMY package [11], [12], [13] represents an average response of the available models and has been used to generate data for the Higgs boson mass scan. Signal events have been generated with both HERWIG and PYTHIA [14] at a Higgs boson mass of 130 GeV to estimate the contribution of this effect to the systematic uncertainty. To generate an invisible Higgs boson sample, the Higgs boson is forced to decay into two Z bosons which are subsequently forced to decay into neutrinos. The set of data samples produced for this analysis is summarized in Table 1. The VBF signal Monte-Carlo was produced to leading order. The difference between LO and NLO cross-section is negligible, $\sim 1\%$[9], therefore the

Higgs boson Mass [GeV]	Cross-section [pb]	# Events	Generator
110	4.63	10k	JIMMY
130	3.96	30k	JIMMY
130	3.93	10k	PYTHIA6.4
200	2.41	10k	JIMMY
250	1.79	10k	JIMMY

Table 1: Invisible Higgs boson samples generated for this analysis. Leading-order cross-sections for the Higgs boson produced via Vector Boson Fusion were evaluated by the ATLAS Higgs Working group [15].

Jet Sample	$\sigma(pb)$	p_T range [GeV]
J0	1.76×10^{10}	8-17
J1	1.38×10^{9}	17-35
J2	9.33×10^{7}	35-70
J3	5.88×10^{6}	70-140
J4	3.08×10^{5}	140-280
J5	1.25×10^{4}	280-560
J6	3.60×10^{2}	560-1120
J7	5.71×10^{0}	1120-2240

Table 2: Cross-section and p_T range for the QCD dijet background samples generated with PYTHIA. The cross-sections given in the second column are for the specific p_T range with no other cuts.

LO cross-sections were been used for the signal in this note. Table 1 includes the Standard Model VBF Higgs boson production cross-section that were used [9].

For an ideal detector, event selection cuts efficiently remove the QCD dijet background. However, this background is considered because of the large cross-section for the process and the presence of poorly instrumented regions and dead regions generating false missing transverse energy (E_T^{miss}) signals. In order to provide enough statistics throughout the full transverse momentum (p_T) spectrum, the QCD background was divided into several p_T ranges to produce several sub-samples, of approximately equal number of events, as shown in Table 2 [16]. The surviving background comes from the high p_T bins allowing reasonable statistics in the final sample. Thus the binning is used to generate the QCD background within a reasonable amount of computer time and allow for the very high rejection factor for this background in this analysis.

In previous ATLAS studies of the invisible Higgs boson produced via the VBF process, the PYTHIA package has been used to generate both the W+jet and Z+jet backgrounds. However, the PYTHIA implementation for these backgrounds only includes the matrix element term for the $q\bar{q} \rightarrow gV$ and $qg \rightarrow qV$ processes. The PYTHIA implementation tends to underestimate the Z+2jets process because it does not include a complete matrix element calculation. In contrast, ALPGEN [17] provides an exact matrix calculation at tree level for up to 3 partons. For this reason, ALPGEN was used to produce both the W+jet and Z+jet backgrounds. Within ALPGEN, there are two different Z+jet implementations, one which only includes QCD matrix element terms and the second which includes the QCD and EW matrix element terms. In the second case, only on-shell bosons are created without Z/γ^* interference, in contrast, the first case does include these effects. By comparing events generated with the two different implementations it was found that the QCD-only process underestimates the background by $\sim$25%. The effect of a non-zero

Z boson width was checked by varying the Z boson mass. This showed that the result was insensitive to the use of on-shell bosons. Therefore, all ALPGEN samples used in this study were generated using the option that included both QCD+EW terms.

For the Z+jet background, three samples were produced for each of the two decay modes, $Z \to \nu\nu$ and $Z \to \ell\ell$. Two exclusive samples were produced for the one and two parton final states and one inclusive sample was produced for three or more partons. Default ALPGEN settings were used to generate events except for a cut to remove very low E_T^{miss} events by setting $E_T^{miss} > 10$ GeV and a change in acceptance to ensure complete η coverage by opening the phase space setting for both jets and leptons ($|\eta_j| < 6$ and $|\eta_\ell| < 6$).

In this study, only the leptonic decay of the W boson from the W+jet background was considered. The E_T^{miss} arises from a combination of the E_T^{miss} associated with the neutrino and the lepton energy in the case where the lepton escapes detection. The W+jet background was generated in the same manner as for the Z+jet background.

2.2 Trigger

The major challenge for triggering candidate events for the VBF invisible Higgs boson analysis is to retain signal events whilst reducing the very large QCD background to an acceptable level. These problems are particularly acute with the first level trigger (L1) which can easily be overwhelmed by the QCD background. A trigger for these signal events is possible using a relatively high E_T^{miss} cut while selecting one or two jets of moderate transverse energy. For triggers of this type, QCD backgrounds dominate. In order to produce an acceptable rate for the High Level Trigger (HLT), the trigger menu items used to select invisible Higgs boson events should add no more than a few Hz of trigger rate, even at the highest luminosities.

The trigger study of this note is based on the standard full ATLAS simulation of the L1 trigger. The HLT has not been considered, as at the time of the study HLT algorithms for E_T^{miss} had not been fully implemented and there had been no simulation of forward jets. Jets are classified into central jets $|\eta| < 3.2$ and forward jets $3.2 < |\eta| < 5$.

Data for the trigger study consisted of the sample of VBF Invisible Higgs boson events with a Higgs boson mass of 130 GeV produced using HERWIG and a sample of QCD dijet produced using PYTHIA as described in Section 2.1. The results of this study are shown in Table 3 for 10^{31} cm^{-2} s^{-1} luminosity. The acceptances shown in Table 3 give the effect of the trigger on the VBF Higgs boson samples used in the VBF analysis. As such the acceptance is defined as the number of signal events that survive both the trigger and the data selection cuts described in Section 2.3.1, divided by the number of events that survive the selection cuts alone. The trigger rates in Table 3 are the expected raw rates for the specific trigger. One expects an overlap with other trigger signatures such that the additional rate produced by these signatures will be less than the calculated raw rates.

The numbers given in Table 3 are the best estimation we currently have of the trigger rates. In reality beam conditions and detector effects could lead to much higher values. It is clear that the trigger strategy will depend on these background effects and on the luminosity. At low luminosities, (10^{31} cm^{-2} s^{-1}) it is likely that a simple trigger based on E_T^{miss} alone such as $E_T^{miss} > 70$ GeV (L1_XE70) will be sufficient. However if the trigger rate for this item is higher than expected, VBF invisible Higgs boson events could still be triggered using a higher E_T^{miss} trigger such as $E_T^{miss} > 80$ GeV (L1_XE80) or $E_T^{miss} > 100$ GeV (L1_XE100) whichever one can be used without pre-scaling. As the luminosity increases or if backgrounds are worse than expected, it will be necessary to use a combined trigger for this channel. The numbers in Table 3 suggest that triggers based on E_T^{miss} and either a forward or central jet would be sufficient. However the addition of a single jet to an E_T^{miss} trigger provides a relatively small reduction in rate due to correlations that can occur when high energy jets are mis-measured. There is concern that this could be amplified by pile-up effects. Requiring a forward jet plus a central jet plus E_T^{miss} is expected to

Trigger Menu	Acceptance[%] normalized to offline cuts	Rates[Hz] for $\mathcal{L} = 10^{31}$ cm^{-2} s^{-1}
L1_XE60	99	5.0 ± 1.3
L1_XE70	98	1.5 ± 0.6
L1_XE80	96	0.6 ± 0.1
L1_XE100	84	0.2 ± 0.1
L1_XE120	70	0.1 ± 0.1
L1_FJ23+XE70	78	0.9 ± 0.6
L1_J23+L1_XE70	83	1.4 ± 0.6
L1_J23+L1_XE100	73	0.2 ± 0.1
L1_FJ23+L1_XE100	66	0.0 ± 0.0
L1_FJ23+L1_J23+L1_XE70	62	0.9 ± 0.6
L1_FJ23+L1_J23+L1_XE100	55	0.0 ± 0.0

Table 3: Signal acceptance and level one trigger rates for the VBF invisible Higgs boson channel based on full ATLAS simulations and with $m_H = 130$ GeV . The L1 trigger menu items are E_T^{miss} (L1_XE) central jet (L1_J) and forward jet (L1_FJ), see text. The number following the menu object indicates the trigger threshold given in GeV. Both single and combined triggers are shown in this Table. The values are given for a luminosity of 10^{31} cm^{-2} s^{-1} and do not account for pile-up effects.

solve these problems albeit with a reduction of signal acceptance. For a luminosity of 10^{33} cm^{-2} s^{-1}, the most conservative trigger option is a combined trigger with $E_T^{miss} > 100$ GeV and a forward and a central jet each with a $p_T > 23$ GeV. This trigger will have an acceptance rate for the signal of 55% as shown in Table 3. Note that the uncertainties shown in Table 3 are statistical only. A further major uncertainty in trigger rates are pile-up effects which have not been considered here. In practice, adjustments will be required to select the optimum trigger based on the experimental rates observed at the LHC.

Invisibly decaying Higgs boson events produced via vector boson fusion can be selected using a combination of E_T^{miss} and jet triggers with a small impact on the overall L1 trigger rate. For low luminosities (10^{31} cm^{-2} s^{-1}) it is expected that a E_T^{miss} trigger of 70 GeV or greater will be sufficient. For higher luminosities such as 10^{33} cm^{-2} s^{-1}, a trigger with $E_T^{miss} > 100$ GeV and a forward and central jet each with $p_T > 23$ GeV will be required.

2.3 Event selection for the VBF channel

Two separate methods are used to extract the signal: the first method is called the cut-based analysis, the second is the shape analysis. Both analyses are conducted by first applying the selection cuts described in the next sub-section. For the cut-based analysis, the signal is extracted using all the cuts including a cut on ϕ_{jj}, the angle between the two tagged jets in the transverse plane. This is described in Section 2.5. For the shape analysis, this last cut is not applied. Instead, the shape of the ϕ_{jj} distribution is used to extract the fraction of signal events. This is described in Section 2.6. Results are derived separately with these two methods.

The selection cuts described in this section were developed using a signal sample with $m_H = 130$ GeV.

2.3.1   Selection cuts

The event selection is based on standard ATLAS definitions for jets, leptons and missing transverse energy [18]. A primary characteristic of a signal event is the presence of two jets from the VBF process. Events are selected based on each of the two highest p_T jets in the event which are referred to as the "tagging jets". These tagging jets are required to have a $p_T > 40$ GeV and be in the rapidity range $|\eta_{j1,2}| < 5$. Cuts on the product and difference of the pseudorapidity of the two jets are used, $\eta_{j1} \cdot \eta_{j2} < 0$ and $\Delta\eta > 4.4$, respectively. Kinematic distributions of the tagged jets for the signal and background are shown in Figure 2. In the upper two plots of this Figure, it can be seen that signal events and the W+jet and Z+jet backgrounds have very similar p_T distributions. When the W+jet and Z+jet events are generated with only one parton the p_T distributions are much softer. When the two parton and three parton components are added the p_T distribution becomes harder and similar to the signal.

The second major event characteristic used to select events is a large E_T^{miss} from the invisible decay of the Higgs boson. A cut on this variable significantly reduces the QCD background as no real E_T^{miss} is expected for QCD events. In this analysis there is a requirement that $E_T^{miss} > 100$ GeV. The E_T^{miss} distributions for the signal and backgrounds are shown in Figure 3.
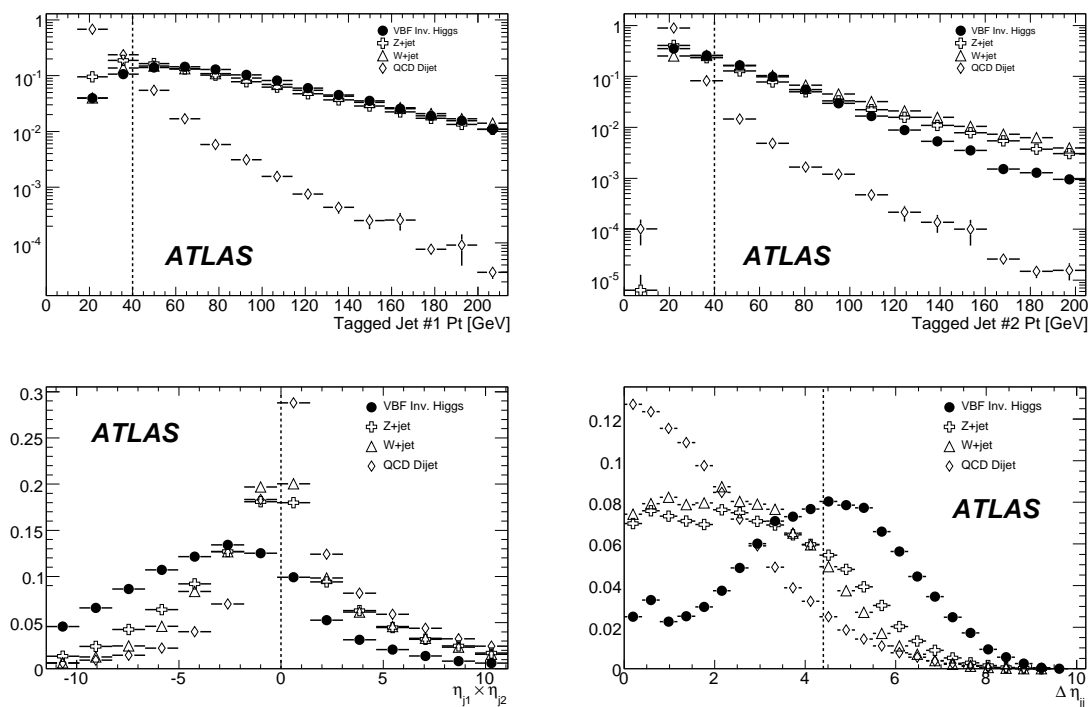

Figure 2: Comparison of tagged jet properties for signal events ($m_H = 130$ GeV) and the three major backgrounds. The upper left plot shows the p_T of the leading tagged jet, the upper right plot shows the p_T of the jet with the second highest p_T. The lower left plot shows the product of the directions of the two tagged jets in pseudo-rapidity ($\eta_{j1} \times \eta_{j2}$), and the lower right plot shows the difference in η between the two tagged jets ($\Delta\eta$). The enhancement at $\Delta\eta$ of 0.5 in the VBF signal results from a single high p_T jet being reconstructed as two jets. The filter cut described in Section 2.1 has been applied to the W+jet and Z+jet Monte-Carlo data, but no trigger cuts have been applied. The distributions are normalized to unity. The vertical dotted lines show the cut values used in the analysis.
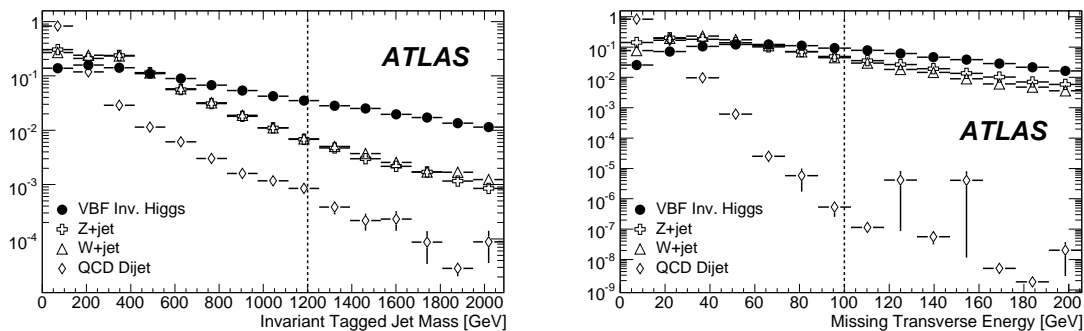
Figure 3: The reconstructed invariant mass of the tagging jets (left) and the E_T^{miss} (right) for the invisible Higgs boson signal ($m_H = 130$ GeV) and the three main backgrounds. Single events in the high E_T^{miss} tail of each individual sample (J0, J1 etc) can result in a spike with a large error. The filter cut described in Section 2.1 has been applied to the W+jet and Z+jet Monte-Carlo data, but no trigger cuts have been applied. The distributions are normalized to unity.

The majority of QCD dijet background events will produce soft jets resulting in the tagging jets having a low invariant mass. This feature can be used to reject QCD events by requiring a minimum invariant mass of 1200 GeV for the tagging jets. The invariant mass distribution of the tagging jets is shown in Figure 3. The QCD dijet background can be further reduced by requiring that the direction of the measured E_T^{miss} is not correlated with the tagging jets. A missing transverse energy isolation variable, I, is defined for this purpose as $I = min[\phi(E_T^{miss}) - \phi(j_{1,2})]$. Events with a small value of I are expected to result from mis-measured jets caused by dead material and cracks in the detector. This is illustrated in Figure 4 which shows that QCD dijet events preferentially have a small value of I. A selection of $I < 1$ rad has been used which is compatible with previous analyses. The W+jet and Z+jet backgrounds can be reduced by rejecting events with any identified lepton. For this reason, events with electrons or muons with a $p_T > 20$ GeV are rejected, as are events containing τ-jets with a $p_T > 30$ GeV. These cuts are based on an earlier ATLAS fast simulation study.
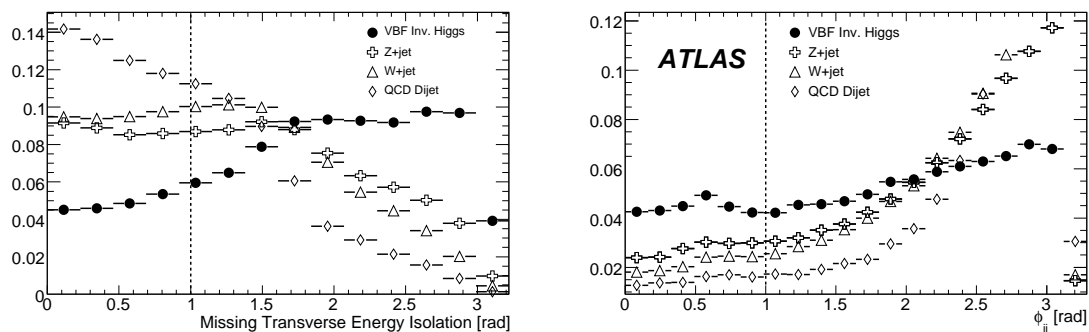
Figure 4: The distribution of the reconstructed E_T^{miss} isolation variable (I) is shown in the right hand plot and the azimuthal angle between the tagging jets (ϕ_{jj}) is shown in the right hand plot for the invisible Higgs boson signal ($m_H = 130$ GeV) and the three main backgrounds. The filter cut described in Section 2.1 has been applied to the W+jet and Z+jet Monte-Carlo data, but no trigger cuts have been applied. The distributions are normalized to unity.

A key aspect of the VBF Higgs boson search is the electroweak nature of the signal, and this can be used to suppress backgrounds by using the fact that the signal has no color flow between the interacting quarks at tree level. Although the W+jet and Z+jet backgrounds include both electroweak and QCD terms, the cross-section is dominated by the QCD contribution. Therefore, unlike the signal, the majority of background events have QCD activity in the central region. The presence of this extra QCD radiation between the two tagging jets provides, in principle, a powerful tool to suppress this background. In practice the difference is diluted both by the underlying event and pile-up. The Underlying Event (UE) arises from interactions of the spectator partons and is not consistently modeled by the available event generators. For example, the ratio of the average jet multiplicity from the UE between HERWIG/PYTHIA is between 1.38 and 1.85. Therefore PYTHIA generates events with fewer jets from the UE, but these jets have on average a higher p_T. If a cut is applied to remove events that have a central jet that exceed a specific p_T value, the so called Central Jet Veto (CJV) cut, fewer PYTHIA events will survive than HERWIG events. Although there is a clear difference in the topology between the signal and background, the added contribution from the UE has a large effect on the efficiency of this cut. In the same way pile-up, which results from central activity unrelated to the event of interest can also reduce the effectiveness of this CJV cut. The effect of pile-up has not been studied, as suitable data samples were not available. For this analysis, a central jet veto is used requiring that there are no additional jets with $p_T > 30$ GeV for $|\eta| < 3.2$. It should be stressed that this cut is applied after the selection of the two tagging jets which can be located anywhere within the full η range including $|\eta| < 3.2$. So this cut does not bias the selection of the tagging jets, nor does it introduce a bias with respect to the trigger which has elements that allow jets to be located within an $|\eta| < 3.2$.

Unlike the signal which is uniquely produced via Vector Boson Fusion, the W+jet and Z+jet backgrounds can be produced by the $q\bar{q} \rightarrow gV$ and $qg \rightarrow qV$ processes in which the second jet comes from a radiative process. Therefore, the difference in ϕ between the two tagged jets is different for the signal and the radiative background as can be seen in Figure 4. This difference provides additional discriminating power and is used in the analysis presented in Section 2.5 requiring $\phi_{jj} < 1$ rad. Moreover, the ϕ_{jj} variable motivates the shape analysis presented in Section 2.6.

The selection cuts along with the surviving cross-sections after each cut are shown in Table 4 for a Higgs boson mass $m_H = 130$ GeV and the three main backgrounds. Table 5 shows the effect of the cuts for the four Higgs boson mass values considered in this study. The cross-sections for W+jet and Z+jet processes were calculated to LO but have been normalized to the results calculated with the generator FEWZ at NNLO which results in a value for the total cross-section which is known to within $\sim 10\%$[1] [19].

The first cut applied to the data simulates the effect of the L1 trigger with the most conservative menu option given in Table 3 and discussed in the previous section namely, a $E_T^{miss} > 100$ GeV, a central jet with $p_T > 23$ GeV and a forward jet with $p_T > 23$ GeV. This cut reduces the QCD dijet background rate by approximately 7 orders of magnitude. The effect of the trigger on the W+jet and Z+jet backgrounds is smaller with a reduction of two orders of magnitude, by contrast the signal is reduced by about 50%. The jet tagging cuts reduces all three backgrounds by a factor of 10. Although a L1 E_T^{miss} is applied a large fraction of events still survive because of the the L1 E_T^{miss} resolution. The other cuts that have a large impact on the QCD rate are the E_T^{miss} cut and the E_T^{miss} isolation cut. Together they reduce this background to a negligible level. The effect of these selection cuts on the Z+jet and W+jet backgrounds are less dramatic. The lepton veto reduces the W+jet and Z+jet by $\sim 36\%$ and $\sim 3\%$, respectively. The lepton veto cut removes few events in the Z+jet channel as the E_T^{miss} cut removes most of the Z$\rightarrow \ell\ell$ decay mode. The remaining Z+jet events are dominated by the Z$\rightarrow \nu\nu$ mode. Leptons are only identified for $|\eta| < 2.5$, so the lepton veto cut does not remove all the W+jet background events due to this limited η range. Therefore, electrons and τ-jet in the forward region ($|\eta| > 2.5$) are mis-identified as jets most

---

[1] This includes the PDF and QCD scale uncertainties.

Selection Cuts	Higgs boson $m_H = 130$ GeV	W+jet	Z+jet	QCD
Initial σ (fb)	3.93×10^3	1.24×10^6	4.08×10^5	1.91×10^{13}
L1 Trigger	2.71×10^2 (0.07)	1.42×10^4 (0.01)	6.31×10^3 (0.02)	1.52×10^6 (<0.01)
+ Tagged jets	1.47×10^2 (0.54)	1.35×10^3 (0.10)	6.16×10^2 (0.10)	1.81×10^5 (0.12)
+ M_{jj}	1.11×10^2 (0.76)	6.64×10^2 (0.49)	3.76×10^2 (0.61)	1.28×10^5 (0.71)
+ $E_T^{miss} > 100$ GeV	1.08×10^2 (0.97)	4.70×10^2 (0.71)	2.69×10^2 (0.72)	2.84×10^3 (0.02)
+ Lepton veto	1.07×10^2 (1.00)	3.01×10^2 (0.64)	2.62×10^2 (0.97)	2.76×10^3 (0.97)
+ $I > 1$ rad	9.60×10^1 (0.89)	1.49×10^2 (0.49)	2.11×10^2 (0.81)	3.61 (<0.01)
+ Central jet veto	8.93×10^1 (0.93)	1.10×10^2 (0.74)	1.32×10^2 (0.63)	0.07 (0.02)
+ $\phi_{jj} < 1$ rad	4.50×10^1 (0.50)	1.94×10^1 (0.18)	4.21×10^1 (0.32)	0.07 (1.00)

Table 4: Cross-section in fb for a Higgs boson ($m_H = 130$ GeV) and background samples at each step of the selection process. Initial cross-section for W/Z+jet are quoted after VBF filter and NNLO corrections. The first cut is the effect of the L1 trigger simulation with a E_T^{miss} of 100 GeV, a central jet with $p_T > 23$ GeV and a forward jet with $p_T > 23$ GeV (Table 3). The central jet veto is applied to jets other than the two tagging jets and does not bias any of the other cuts. Numbers in parentheses are the efficiencies for each cut.

Higgs boson mass [GeV]	100	130	200	250
Initial $\sigma(fb)$	4630	3930	2410	1780
L1 Trigger	322	271	240	168
+ Tagged jets	166	147	134	93
+ M_{jj}	126	111	100	73
+ $E_T^{miss} > 100$ GeV	121	108	98	70
+ Lepton veto	121	107	98	70
+ $I > 1$ rad	108	96	86	63
+ Central jet veto	94	89	79	59
+ $\phi_{jj} < 1$ rad	43	45	39	30

Table 5: Cross-section in fb for each signal mass at each step in the selection cuts. The first cut is the effect of the L1 trigger simulation with a E_T^{miss} of 100 GeV, a central jet with $p_T > 23$ GeV and a forward jet with $p_T > 23$ GeV.

of the time. In a similar manner, muons in the forward direction are generally not identified and result in fake E_T^{miss}.

2.4 Systematic uncertainties

Three major types of systematic uncertainties are considered. One arises from the implemention of the Monte Carlo generators, the second from the experimental systematic uncertainties and the third from the theoretical knowledge of the production cross-sections.

Two event generator effects are discussed, the first is the treatment of the Underlying Event (UE) and the second is the effect of using a fixed Z boson mass. To illustrate the effect of the UE, signal events have been generated with two different event generators, HERWIG and PYTHIA that treat the UE in different ways. Table 6 shows the efficiency of each selection cut used in the VBF analyses for the two generators. The difference in cross-sections between the two samples are within $\sim 2\%$ of each other for cuts up to the E_T^{miss} isolation cut. However, once the central jet veto is applied, fewer Pythia events

Selection Cuts	HERWIG 130 GeV	PYTHIA 130 GeV
Initial $\sigma(fb)$	3.93×10^3 (1.000)	3.93×10^3 (1.000)
Pre-Cut (E_T^{miss} > 80 GeV)	1.76×10^3 (0.448)	1.78×10^3 (0.453)
+ Tagged Jets	4.07×10^2 (0.231)	4.10×10^3 (0.230)
+ M_{jj}	2.45×10^2 (0.602)	2.45×10^3 (0.598)
+ E_T^{miss} > 100 GeV	2.05×10^2 (0.837)	2.14×10^3 (0.873)
+ Lepton Veto	2.05×10^2 (1.000)	2.12×10^2 (0.991)
+ $I > 1\ rad$	1.84×10^2 (0.898)	1.80×10^2 (0.849)
+ Central Jet Veto	1.59×10^2 (0.864)	1.07×10^1 (0.594)
+ $\phi_{jj} < 1\ rad$	7.43×10^1 (0.467)	4.93×10^1 (0.461)

Table 6: Comparison between HERWIG and PYTHIA generated samples on the selection cuts for the 130 GeV Higgs boson mass. The cross-section results are quoted in fb and the cut efficiency is given in parenthesis. The major difference occurs in the last two rows of this table.

survive resulting in a large difference of $\sim 49\%$. This is believed to be the result of the difference in the modeling of the UE in the two generators; Pythia tends to produce fewer but harder jets, resulting in more events being removed by the central jet veto cut, see Section 2.3. If the number of background events is underestimated due to a combination of this cut and the choice of generator the sensisitivity to the signal will be artificially enhanced. A systematic study of the effect of generator choice on the central jet veto cut would require a large number of data and background samples to be produced with a variety of generators and this is beyond the scope of this paper. It is not clear which generator represents reality best. For consistency both the background and signal samples were generated using HERWIG. When real data becomes available it will be possible to measure the magnitude of central jet activity directly and use this to tune the generators.

The use of ALPGEN requires the use of a fixed Z mass. The effect of the missing off-shell terms from the background samples was checked using the $Z \rightarrow \nu\nu$ analysis by adding a E_T^{miss} contribution randomly generated by a Breit-Wigner distribution using the Z mass and width parameters. This study indicated that the effect of using a fixed mass Z boson was negligible.

Two methods are considered in this paper to extract the signal significance. The first, a cut-based analysis, relies on the number of signal and background events after all cuts have been made. The second, a shape analysis relies on the ratio of the number of background events contained in two regions of the ϕ_{jj}variable distribution; namely the number of events for $\phi_{jj} < 1$ divided by all events. The systematic uncertainties of interest are the ones related to these three quantities; the number of signal and background events and the background shape ratio. They are shown in Table 7.

The event reconstruction variables that result in the largest systematic uncertainties are the jet resolution and the jet energy scale. For the jet energy resolution, the systematic uncertainty was estimated by smearing the momentum of the jets using a Gaussian distribution with a width given by $\sigma(E) = 0.45\sqrt{E}$ for $|\eta| < 3.2$ and $\sigma(E) = 0.63\sqrt{E}$ for $|\eta| > 3.2$. Changing the jet energy magnitude also affects the E_T^{miss}, so for each event, E_T^{miss} was recalculated for the x- and y-components. The analysis was then repeated to determine the change in the number of signal and background events and the shape ratio. In the same way the effect of changes in the jet energy scale was investigated by shifting the overall scale by $\pm7\%$ for $|\eta| < 3.2$ and $\pm15\%$ for $|\eta| > 3.2$. Again this affects the E_T^{miss}, and this change was taken into account. As can be seen in Table 7, there is an asymmetric dependence on the jet energy scale, so positive and negative deviations are considered separately. Lepton reconstruction was analyzed and found not to contribute to the final systematic uncertainty. The JES uncertainties used here are conservative for

Systematics	Higgs boson 130 GeV	Background	
		Cut-Based	Shape
Luminosity	3 %		$\sim 0\%$
Jet energy resolution: $\sigma(E) = 0.45\sqrt{E}$ for $|\eta| < 3.2$ $\sigma(E) = 0.63\sqrt{E}$ for $|\eta| > 3.2$	0.8 %	5.3 %	4.5 %
Jets energy scale: $+7\%$ for $|\eta| < 3.2$ $+15\%$ for $|\eta| > 3.2$	4.0 %	3.2 %	0.2 %
Jets energy scale: -7% for $|\eta| < 3.2$ -15% for $|\eta| > 3.2$	10.0 %	19.5 %	2.8 %
Total	10.5 %	20.4 %	5.3 %

Table 7: Experimental contributions to the systematic uncertainty. The systematic uncertainty on the Jet Energy Scale (JES) is asymmetric. Only the largest (negative) JES systematic uncertainty is included in the total experimental uncertainty shown in the last row of the table.

30 fb^{-1}, but the impact of this choice on the sensitivity limits presented in this paper is small. Finally, 3% was assigned to the uncertainty in the luminosity. To get the experimental systematic uncertainty for each analysis the terms were added in quadrature giving an overall systematic uncertainty of 20% on the number of background events which applies to the cut-based analysis and an uncertainty of 5.3% on the background shape ratio that applies to the shape analysis.

In addition to the uncertainty in the UE and the reconstruction algorithms, there is a systematic uncertainty which arises from the uncertainty in the absolute cross-section of the backgrounds. The main backgrounds to the invisible Higgs boson channel are Z+jet and W+jet. The total cross-sections for these processes have been corrected to NNLO and are known to $\sim 10\%$, (see Section 2.3). However the cuts used to select the VBF process, result in a very restricted phase space which makes it difficult to determine the systematic uncertainty on the cross-section for the final data samples. This means that the systematic uncertainty on the number of background events due to the cross-section is currently unknown, could be very large and is likely to dominate other uncertainties. The shape of the ϕ_{jj} distribution on the other hand is quite well constrained by theory and based on previous studies has a systematic uncertainty of 10% [5]. At NLO it is expected to be 5%. In this analysis a conservative value of 10% is assumed for the uncertainty due to the cross-section which when combined with the much smaller experimental effect leads to an overall systematic uncertainty of 11.3% on the background shape.

2.5 Cut-based analysis

This analysis uses the selection cuts summarized in Section 2.3.1. The signal significance is calculated based on the number of signal and background events that remain after all cuts. The limitation of this analysis is that the systematic uncertainty on the background cross-sections described in the previous section could be very large. One way of dealing with this uncertainty is to use experimental data of the Z+jet channel where the Z decays to two leptons. After correction for the detector acceptance, these events can be used to infer the value of the cross-section for the irreducible background in which the Z decays to two neutrinos. A similar analysis can be done for the W+jet background. These so called "data driven" corrections will be the subject of a future publication. In the next section we report on an

alternative method which uses the shape of the azimuthal angle distribution between the jets to reduce the dependence of the systematic error on the cross-section. In the current section the sensitivity to an invisible Higgs boson without systematic errors are calculated to provide baseline numbers for the sensitivity to an invisible Higgs boson produced via the VBF process.

The number of signal and background events after the ϕ_{jj} cut is shown in Tables 4 and 5. These numbers can be used to calculate the 95 % CL sensitivity of ξ^2 for the invisible Higgs boson, given the assumed backgrounds. This is done by calculating the number of signal events required to increase the total event count by a factor 1.64 times the uncertainty on the number of background events as shown in Equation 2.

$$1.64\sigma_B = N_S\xi^2 \tag{2}$$

Here N_S is the number of signal events after the selection cuts and $\sigma_B = \sqrt{N_B}$. The results of this analysis gives a ξ^2 for an integrated luminosity of 30 fb^{-1}at 95 % C.L. for Higgs mass between 110 GeV and 250 GeV of $\sim 5 - 8\%$ in the case when systematic uncertainties are not included. An additional 6% statistical uncertainty[2] arises from the limited number of events in the data samples.
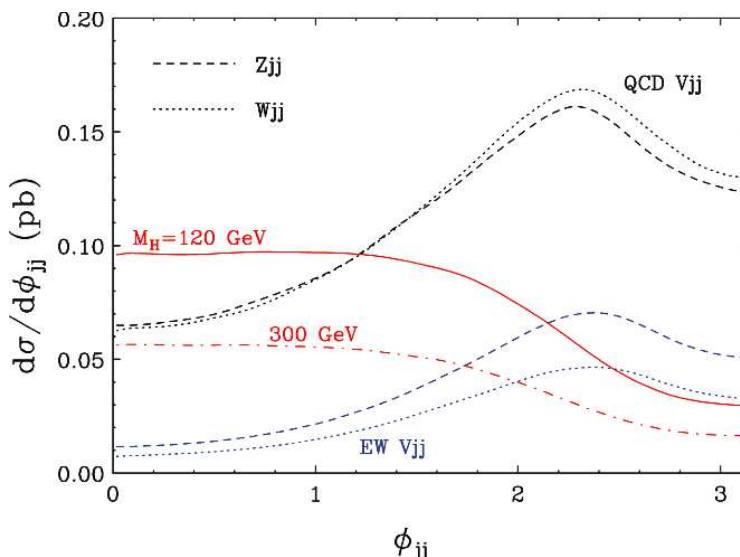
2.6   Shape analysis

Figure 5: The ϕ_{jj} distribution for the signal and background in radians [5]. The solid and dash-dotted lines represent the expected distribution for the Higgs boson signal with Higgs boson masses of $m_H = 120$ and $m_H = 300$ GeV respectively. The dotted and dashed lines represent the distributions expected from the backgrounds. The plot shows the distributions after VBF selection cuts have been made. Note that for the ϕ_{jj} plot shown earlier did not have these cuts applied, (Figure 4).

The shape analysis is motivated by a marked difference in the ϕ_{jj} distribution between the signal and the W/Z+jet background as shown in Figure 5, which is taken from reference [5]. This plot shows that the backgrounds peak above a ϕ_{jj} of 1 while the signal is higher at low ϕ_{jj} values. To characterize the shape of the ϕ_{jj} distribution the ratio R has been defined as the number of events with $\phi_{jj} < 1$ divided by

---

[2]Based on a binomial error calculation.

the total number of events as shown in Equation 3. As the proportion of signal in the sample increases the value of R increases.

$$R = \frac{\int_0^1 \frac{d\sigma}{d\phi_{jj}}}{\int_0^\pi \frac{d\sigma}{d\phi_{jj}}} \tag{3}$$

The advantage of the shape analysis described in this section over other analyses is that it does not require a knowledge of the absolute cross-section but rather the ratio of the number of events for ($\phi_{jj} < 1$) to all events. As such, the systematic error associated with the absolute cross-section is reduced to a negligible amount. However, as discussed in Section 2.4, there is a systematic uncertainty associated with the knowledge of the ϕ_{jj} distribution which is known to ~10% or better. In addition, the systematic uncertainties due to detector effects are much smaller for this ratio than they are for the number of background events, which is the relevant variable for a pure cut-based analysis (Table 7). The overall systematic uncertainty on the ratio R has been calculated to be 11.3%.

Equation 3 can be re-written in the context of this analysis and expanded to provide a background-only term, as shown in Equation 4.

$$R = \frac{N_B^1}{N_B^\pi} \left[1 + \xi^2 \left(\frac{N_S^1}{N_B^1} - \frac{N_S^\pi}{N_B^\pi} \right) + \cdots \right] \tag{4}$$

Here N_B^1 and N_S^1 are the number of events within $\phi_{jj} < 1$ and N_B^π and N_S^π are the number of events within the entire ϕ_{jj} range. The first term of Equation 4 provides the expected ratio for the background contribution. However, since the ratio between the signal and background are not the same in the presence of a signal, a non-zero value is expected in the second term. The variation from the 'background only' ratio dictates the sensitivity to new physics. The ratio N_B^1/N_B^π can be determined using the Stndard Model theoretical prediction or by a data driven technique.
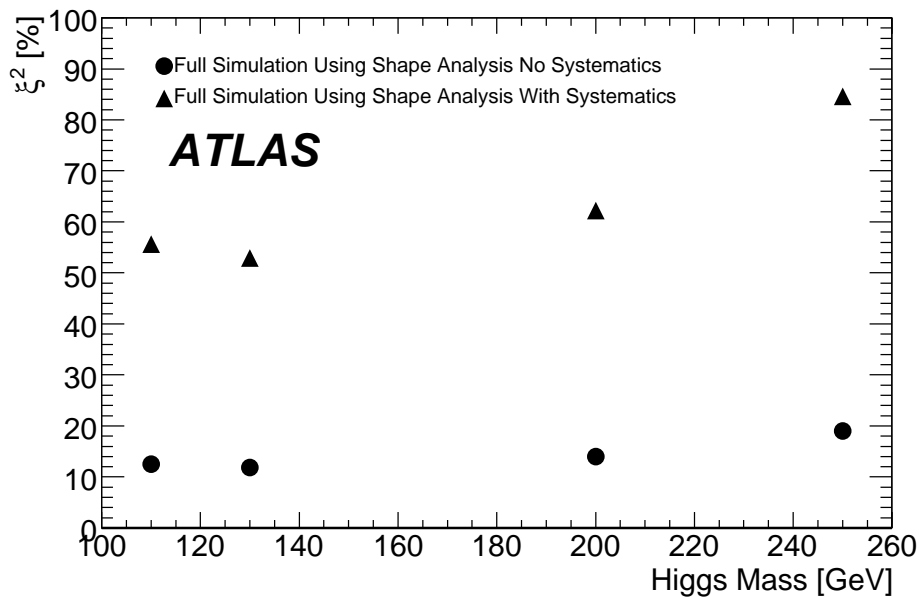

Figure 6: Sensitivity for an invisible Higgs boson at 95% C.L. via the VBF channel using shape analysis for an integrated luminosity of $30 fb^{-1}$ with and without systematic uncertainties. The black triangles (circles) are the results from this analysis with (without) systematic uncertainties.

The shape analysis applies the selection cuts discussed in Section 2.3.1 but not the ϕ_{jj} cut. Therefore, the results from Table 4 before this last cut are used. The first term of Equation 4 is calculated to be 0.254 ± 0.007. To determined the 95% C.L. sensitivity limit a variation of $1.64\sigma_R$ is required, where σ_R is the uncertainty on the ratio R from Equation 4. Therefore, the first order ξ^2 terms from Equation 4 is set to the required 95% CL sensitivity limit, that is $1.64\sigma_R$, as shown in Equation 5.

$$1.64\sigma_R = \xi^2 \left(\frac{N_S^1}{N_B^1} - \frac{N_S^\pi}{N_B^\pi} \right) \left(\frac{N_B^1}{N_B^\pi} \right) \tag{5}$$

Solving for ξ^2 provides the 95 % CL sensitivity limit for the invisible Higgs boson. The results of this analysis are shown in Figure 6. Without systematic errors, the shape analysis gives a value of ξ^2 that ranges from 11 to 19%. This can be compared with the simple cut-based analysis which gave a ξ^2 value that ranged from 5 to 8%. So although the shape analysis method removes the dependence on the absolute cross-section of the backgrounds there is a reduction in the sensitivity to the signal. To include the systematic uncertainties, the uncertainty on the background becomes $\sigma_R = \sqrt{\sigma_R^2 + \alpha^2 R^2}$, where α is the fractional systematic uncertainty given in Table 7. The result obtained that includes systematic uncertainties gives value of ξ^2 of around 60% for m_H between 100 and 200 GeV. This sensitivity is dominated by the systematic uncertainty that arises from the theoretical knowledge of the shape of the ϕ_{jj} distribution. Using calculations at NLO could reduce this uncertainty by a factor of 2 greatly enhancing the sensitivity of this method of analysis.

2.7   Summary for the VBF invisible Higgs boson channel

The study described above has investigated the sensitivity of the ATLAS detector to a Higgs boson particle produced by the VBF process that has an invisible decay mode. It should be stressed that these results do not include pile-up which can reduce the sensitivity. It has been shown that with 30 fb^{-1} of data it is possible to detect this process over a wide range of masses if the Beyond Standard Model cross-section is more than 60% of the Standard Model cross-section for a Higgs mass range of up to 200 GeV and 100% of the Higgs boson decays are invisible. Triggering for this channel is possible using a trigger requiring large E_T^{miss} plus a forward and a central jet of moderate p_T. Triggers of this kind would be useful up to luminosities of at least 10^{33} cm^{-2} s^{-1}.

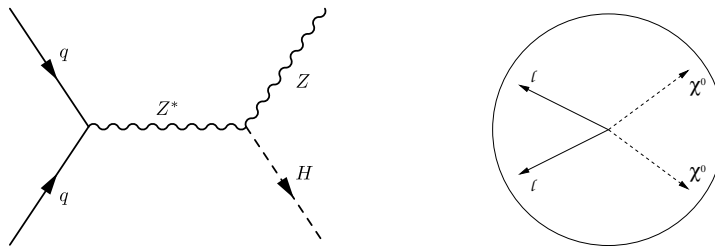# 3   The associated *ZH* production channel

Figure 7: (Left): The Feynman diagram for Higgs boson associated production with a Z boson. (Right): A representation of the decay of a Higgs boson into two invisible neutralinos represented by χ^0 recoiling against the two leptons coming from the *Z* decay.

The Feynman diagram for associated production in the ZH channel is shown in Figure 7. The signal of an invisibly decaying Higgs boson in the *ZH* channel can be detected when the *Z* boson decays into

two leptons, which can be used for triggering the event. The presence of an invisibly decaying Higgs boson is detected from the missing transverse energy.

Various backgrounds with signatures similar to the signal have been studied and are listed here. In all cases, unless otherwise specified, ℓ represents e or μ.

1. The $ZZ \rightarrow \ell\ell\nu\nu$ final state gives the same signature as the signal (irreducible background) and is the main background;

2. The $t\bar{t} \rightarrow b\ell^+\nu\bar{b}\ell^-\nu$ process mimics the signal when the two b-jets are not reconstructed, or when a second lepton results from a b quark decay;

3. The $W^+W^- \rightarrow \ell\nu\ell\nu$ process mimics the signal but can be greatly reduced by cutting on the Z mass;

4. The $ZZ \rightarrow \nu\bar{\nu}\tau\bar{\tau}$ and $\tau \rightarrow \ell\nu\bar{\nu}$ can also mimic the signal.

5. The $ZZ \rightarrow \ell\bar{\ell}\tau\bar{\tau}$ and $\tau \rightarrow \ell\nu\bar{\nu}$ can pass the selection criteria if some particles are missed;

6. The $ZW \rightarrow \ell\ell\ell\nu$ decay mode also simulates the signal when one lepton is not detected;

7. The Z plus jets background, with $Z \rightarrow \ell\bar{\ell}$ (Drell-Yan process) final state can be mistaken for the signal when poor jet reconstruction leads to missing transverse energy.

3.1 Monte Carlo generation for the ZH channel

The signal and the background events have been generated using different particle generators chosen according to which process they simulate best. The events are fully simulated then reconstructed using ATHENA. The diboson production cross-sections are taken from Ref. [19]. All events were passed through a filter immediately after generation. The two filters used are described in detail in Section 3.2.2. Only the few samples generated with the simpler lepton filter will be mentioned here. All other samples were generated with the filter containing m_Z and E_T^{miss} cuts.

Details on the generated events and pre-defined parameters are given below. All generators use the CTEQ6M structure functions to generate the processes.

- Seven signal samples were generated using PYTHIA, with $m_H =$ 110, 120, 130, 140, 150, 200 and 250 GeV. Only the samples with $m_H =$ 130 and 140 GeV used the lepton filter. To generate the invisibility of the Higgs boson, the H is produced as a stable particle, which goes undetected.

- $ZZ \rightarrow \ell^+\ell^-\nu\bar{\nu}$ is generated using PYTHIA. This is the main and irreducible background. One Z decays to a lepton pair while the other is allowed to decay to any flavor of neutrino pairs.

- $t\bar{t}$ is produced with the MC@NLO generator with all top quark decay modes allowed. The filter described in detail in Section 3.2.2 retains mostly $t\bar{t} \rightarrow b\ell^+\nu\bar{b}\ell^-\bar{\nu}$ events with $\ell = e$ or μ only. Hadronic top quark decays with a subsequent $b \rightarrow c\ell\nu$ decay are also included.

- $W^+W^- \rightarrow \ell^+\nu\ell^-\nu$ is generated with MC@NLO.

- $ZZ \rightarrow \tau^+\tau^-\nu\nu$ and $ZZ \rightarrow \ell\ell\tau^+\tau^-$ events are generated with PYTHIA. The τ was allowed to decay hadronically and leptonically in both samples.

- $ZW^\pm \rightarrow \ell^+\ell^-\ell^\pm\nu$ samples are produced with the MC@NLO generator. Since the cross-sections for ZW^+ and ZW^- production are different, two different datasets were generated. The ZW samples were not filtered since MC@NLO does not include the Z width at generation, leading to

problems when trying to apply a cut on the Z mass at the generator level. For these datasets, we use samples generated with the lepton filter which selected events containing at least two leptons. These events need to be reweighted after full reconstruction to account for the distorted Z mass distribution.

- $Z \to \ell^+ \ell^- + jet$ events are produced using the SHERPA generator.

3.2 Event selection for ZH channel

The event selection is made in three stages:

1. For simulated samples, a filter is applied immediately after the event Monte Carlo generation to avoid unnecessary simulation of a large fraction of the background which would otherwise be readily rejected at the preselection level. The event filter cuts are loose preselection cuts applied on true Monte Carlo quantities.

2. The preselection cuts use fully reconstructed variables and aim at rejecting most backgrounds, retaining only the most likely events to be used at the final selection level.

3. The final selection uses a multivariate analysis (Boosted Decision Tree) to refine the selection cuts while retaining a high signal efficiency.

3.2.1 Analysis framework for the ZH channel

The standard ATLAS selection criteria are used to identify these objects [18].

3.2.2 Filter for the ZH channel

The filter decision is based on true Monte Carlo quantities. The filter must not reject events that would have passed the preselection cuts to avoid introducing biases, and must have a large rejection efficiency against background. To do so, the filter uses cuts looser than, but similar to, the preselection cuts, namely:

- The events must contain at least two leptons with $p_T >$ 4.5 GeV of same flavor but opposite charge within $\eta < 2.7$.

- The reconstructed mass of these two leptons must be within ± 25 GeV of the Z mass.

- The events must satisfy $E_T^{miss} > 50$ GeV. The E_T^{miss} is computed from a vectorial sum over all invisible, stable particles such as Higgs bosons and neutrinos, and all lost particles falling outside the calorimeter fiducial region of $p_T > 5.0$ GeV and $\eta > 5.0$.

A simpler lepton filter with only the first selection cut was used for the $ZW \to \ell\ell\ell\nu$ samples, for two signal samples with Higgs mass hypothesis $m_H = 130$ and 140 GeV, and for the $ZZ \to \ell\ell\ell\ell$ sample used for a normalization study.

The filter reduces the total CPU time needed for full reconstruction by more than a factor of 1000. The results are summarized for a signal with a Higgs boson mass hypothesis of 130 GeV and the background samples in Table 8. In Table 9, the effect of the filter, trigger and preselection cuts are shown for the signal at other Higgs boson masses.

channel	$ZH \to \ell\bar{\ell}$ inv. m_H=130 GeV	ZZ $\ell\bar{\ell}\nu\nu$	$t\bar{t}$	WW $\ell\nu\ell\nu$	ZZ $\tau\tau\nu\nu$	ZZ $\ell\ell\tau\tau$	ZW $\ell\ell\ell\nu$	Z+jet $\ell\ell + jet$
# of generated events	10 K	50 K	104 K	70.4 K	50 K	50 K	250 K	27.25K
filter efficiency	75.4%	29.2%	1.13%	4.5%	5.16%	71.4%	100%	0.0154%
σ*BR (fb)	46.2	728.0	833000.0	5245.6	364.0	123.0	820.0	3105063
filter cuts	34.9	212.6	9412.9	236.5	18.8	87.8	820.0	478.4
after trigger	32.5	198.5	8620.6	217.1	14.2	77.8	735.3	460.6
$E_T^{miss} > 90$ GeV cut	14.0	83.8	3254.5	46.6	1.9	4.1	85.9	105.8
p_T lepton cut	10.1	61.6	1596.2	30.5	0.4	1.5	24.0	46.2
$m_Z \pm 20$ GeV cut	9.6	60.2	1187.4	19.9	0.0	1.2	19.7	43.2
b-tag cut	9.3	58.6	358.0	18.7	0.0	1.1	19.0	17.7

Table 8: Monte Carlo estimates of the cross-section times branching ratio in (fb) for the signal with $m_H = 130$ GeV and background processes following successive preselection cuts described in Section 3.2.4 for the ZH analysis. The number of generated events refers to filtered events. The cross-sections are given at NLO as calculated in Ref. [19] for Standard Model processes and from Ref. [9] for the ZH production cross-sections.

	$ZH \to \ell\bar{\ell}$ inv.						
m_H (GeV)	110	120	130	140	150	200	250
# of generated events	10 K	50 K	10 K	10 K	10 K	10 K	10 K
filter efficiency	47.0%	49.6%	75.4%	75.9%	56.4%	64.6%	70.1%
σ·BR (fb)	77.3	59.4	46.2	36.6	29.1	11.0	5.2
after filter cuts	36.3	29.4	34.9	27.7	16.4	7.1	3.6
after trigger cuts	34.0	27.8	32.5	26.0	15.6	6.8	3.5
after $E_T^{miss} > 90$ cut	18.3	15.6	14.0	12.5	10.0	4.9	2.7
after p_T lepton cut	13.5	11.6	10.1	9.3	7.4	3.7	2.0
after $m_Z \pm 20$ GeV cut	13.2	11.4	9.6	8.7	7.3	3.6	2.0
after b-tag cut	13.0	11.1	9.3	8.5	7.1	3.5	2.0

Table 9: Monte Carlo estimates of the cross-section (fb) for the signal with seven different Higgs mass hypotheses following successive preselection cuts described in Section 3.2.4 for the ZH channel analysis. The number of generated events refers to filtered events. Two samples were generated using a simpler filter that retained events containing at least two leptons, ($m_H = 130$ and 140 GeV) whereas all other samples used a filter that required finding two leptons forming a Z boson and large E_T^{miss}, as described in Section 3.2.2. The efficiency for this filter increases with the Higgs mass hypothesis.

3.2.3   Trigger for ZH channel

An invisibly decaying Higgs boson in the *ZH* channel can be detected when the *Z* decays into two leptons. We trigger on such events using the full simulation of the trigger and by requiring either one or two isolated, high p_T leptons satisfying any of the following trigger signatures:

- single electron trigger: one isolated lepton with $p_T > 22$ GeV.

- single muon trigger: one muon with $p_T > 20$ GeV.

- di-electron trigger: two isolated electrons with $p_T > 15$ GeV.

- missing transverse energy trigger: $E_T^{miss} > 100$ GeV.

The di-muon trigger with a lower p_T momentum cut was not implemented in this analysis but will be used in the future. The overall trigger efficiency of 92.8% compares well with what is retained when applying cuts on fully reconstructed variables, selecting events containing either one electron with $p_T > 25$ GeV, two electrons with $p_T > 15$ GeV or one muon with $p_T > 20$ GeV. The effect of the trigger on all samples studied is given in Table 8.

3.2.4   Event preselection

A first preselection is applied to reject most backgrounds, in particular the $t\bar{t}$ and (Z+jet) backgrounds. The following cuts are applied:

- the event must satisfy one of the trigger signatures described in the previous section;

- large missing transverse energy, i.e. $E_T^{miss} > 90$ GeV.

- the event must contain exactly two leptons of the same flavor but opposite charge with $p_T > 15$ GeV;

- an anti-b-tag is applied to further suppress the $t\bar{t}$ background.

- a loose cut on the invariant mass of the two leptons, namely $|m_{\ell\ell} - m_Z| < 20$ GeV, is applied to reject some $t\bar{t}$ background without reducing the signal efficiency.

The $\sigma \cdot BR$ for the signal and the background processes listed in Section 3 are shown in Table 8. The effects of the filter and preselection cuts are also shown in this table.

3.2.5   Final event selection

In order to improve the sensitivity of this channel, the most discriminative variables are used to form a multivariate analysis (Boosted Decision Tree or BDT). Sixteen different variables are used as inputs to the BDT, namely:

- the missing transverse energy E_T^{miss},

- the transverse mass $m_T = \sqrt{2 p_T^{\ell\ell} \cdot E_T^{miss} (1 - \cos \Delta\phi)}$ where $\Delta\phi$ is the azimuthal angle between the dilepton system and $\vec{p}_T^{\;miss}$,

- the cosine of the angle between $\vec{p}_T^{\;miss}$ and the most energetic lepton,

- the reconstructed Z mass,

- the transverse momentum of each lepton,

- the cosine of the angle between the two leptons in the transverse plane and in 3-dimensions,

- the cosine of the angle between $\vec{p_T}^{miss}$ and $\vec{p_T}^Z$,

- the cosine of the angle between the most energetic jet and $\vec{p_T}^{miss}$,

- the energy found in a cone $\Delta R = 0.1$ rad around each lepton; the lepton isolation variable is particularly useful for muons where very little energy is found around isolated muons but not so much for electrons where the energy deposit is much wider,

- the energy of each of the three most energetic jets, and

- the total number of jets.

These variables are shown in Figures 8 to 11 for the signal and the background after applying the preselection cuts listed in Section 3.2.4. Each distribution has been normalized to unity. The various backgrounds have been regrouped: the irreducible background, $ZZ \rightarrow \ell\ell\nu\nu$, the non-resonant background: $t\bar{t}$ and WW, and finally all other backgrounds containing at least one Z boson: $ZZ \rightarrow \ell\ell\tau\tau$, $ZZ \rightarrow \tau\tau\nu\nu$, ZW and $(Z + jet)$.

Each of the main backgrounds after the preselection cuts, namely $t\bar{t} \rightarrow b\ell\nu \; b\ell\nu$, $WW \rightarrow \ell\nu\ell\nu$, $ZZ \rightarrow \ell\ell\tau\tau$, $ZW \rightarrow \ell\ell\ell\nu$ and (Z+jet) are compared to the signal to train a Boosted Decision Tree (BDT) [20]. Each one of these backgrounds is trained separately. Nothing is gained from training a BDT against the irreducible background, $ZZ \rightarrow \ell\ell\nu\nu$, so this background is not used. An ensemble (forest) of decision trees is successively generated from the training sample, where each new tree is trained by giving increased weights to the events that have been misclassified in the previous tree. The classifier response is obtained as the sum of the classification results for each tree, weighted by the purity obtained for all training events in that tree. The large number of decision trees in the forest increases the performance of the classifier and stabilizes the response with respect to statistical fluctuations in the training sample.

For each background type, a set of weights is established. Half the Monte Carlo events contained in each file is used for the training and the other half for the analysis. The file containing the signal and all the backgrounds, including the less important ones, is then analyzed using these weights. Each event is assigned a weight corresponding to the likelihood of being identified as signal or background. The BDT weight distributions are shown in Figure 12. Each plot shows the output variable distribution for Boosted Decision Trees trained against different backgrounds, namely, from top plot to bottom plot, the $t\bar{t} \rightarrow b\ell\nu b\ell\nu$, $WW \rightarrow \ell\nu\ell\nu$, $ZZ \rightarrow \ell\ell\tau\tau$, $ZW \rightarrow \ell\ell\ell\nu$ and Z+jet. The $ZZ \rightarrow \tau\tau\nu\nu$ background is not used to train a specific BDT since too few events survive the preselection cuts. The cuts on the five BDT outputs are adjusted to minimize the value of ξ^2, defined in Equation 2.

The same procedure is repeated using different Higgs boson mass hypotheses ranging from $m_H = 110$ GeV to $m_H = 250$ GeV, optimizing the cuts each time. The numbers of events surviving all Boosted Decision Trees cuts for each Monte Carlo sample and these seven Higgs boson mass hypotheses are given in Table 11. The BDT inputs variables are also ranked during each training against a particular background. Each time, the input variables are assigned a weight proportional to their importance in separating power. The sum of these weights are given in Table 10, showing which variables offer the best separation power. The order of importance varies for each of the trees but all variables are useful in at least one tree. The Z mass is the overall most discriminative variable, mostly due to its very high ranking in the BDT trained against $t\bar{t}$ and WW backgrounds.
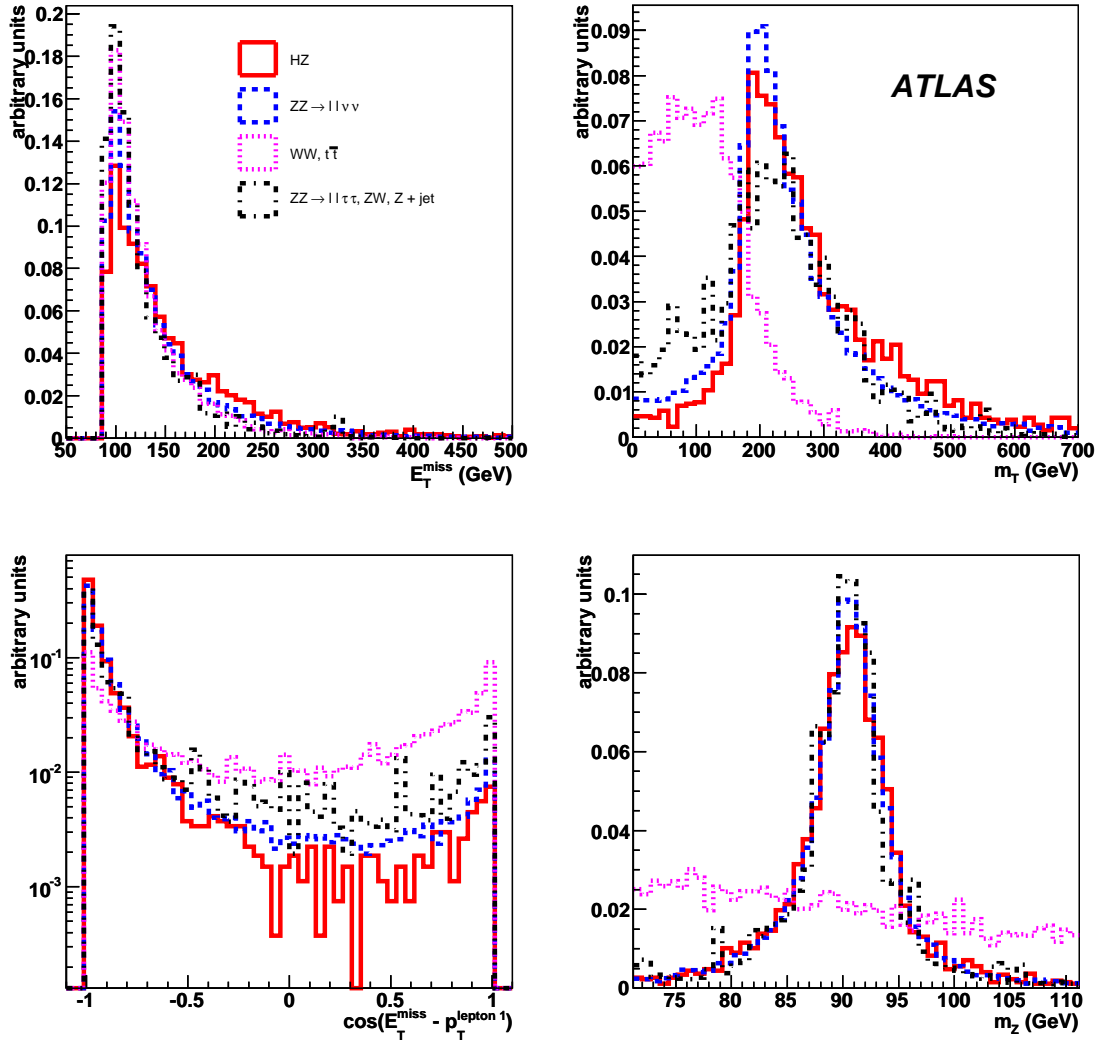
Figure 8: Input variables used by the Boosted Decision Tree for the signal with $m_H = 130$ GeV and the main backgrounds. Top left: Missing E_T. Top right: transverse mass, defined as the reconstructed mass in the transverse plane, namely $m_T^2 = E_T^2 - p_T^2$. Bottom left: cosine of the angle between the missing E_T and highest momentum lepton in the transverse plane. Bottom right: reconstructed Z mass. Each plot has been normalized to unity. The combined samples had first been scaled to the same luminosity.
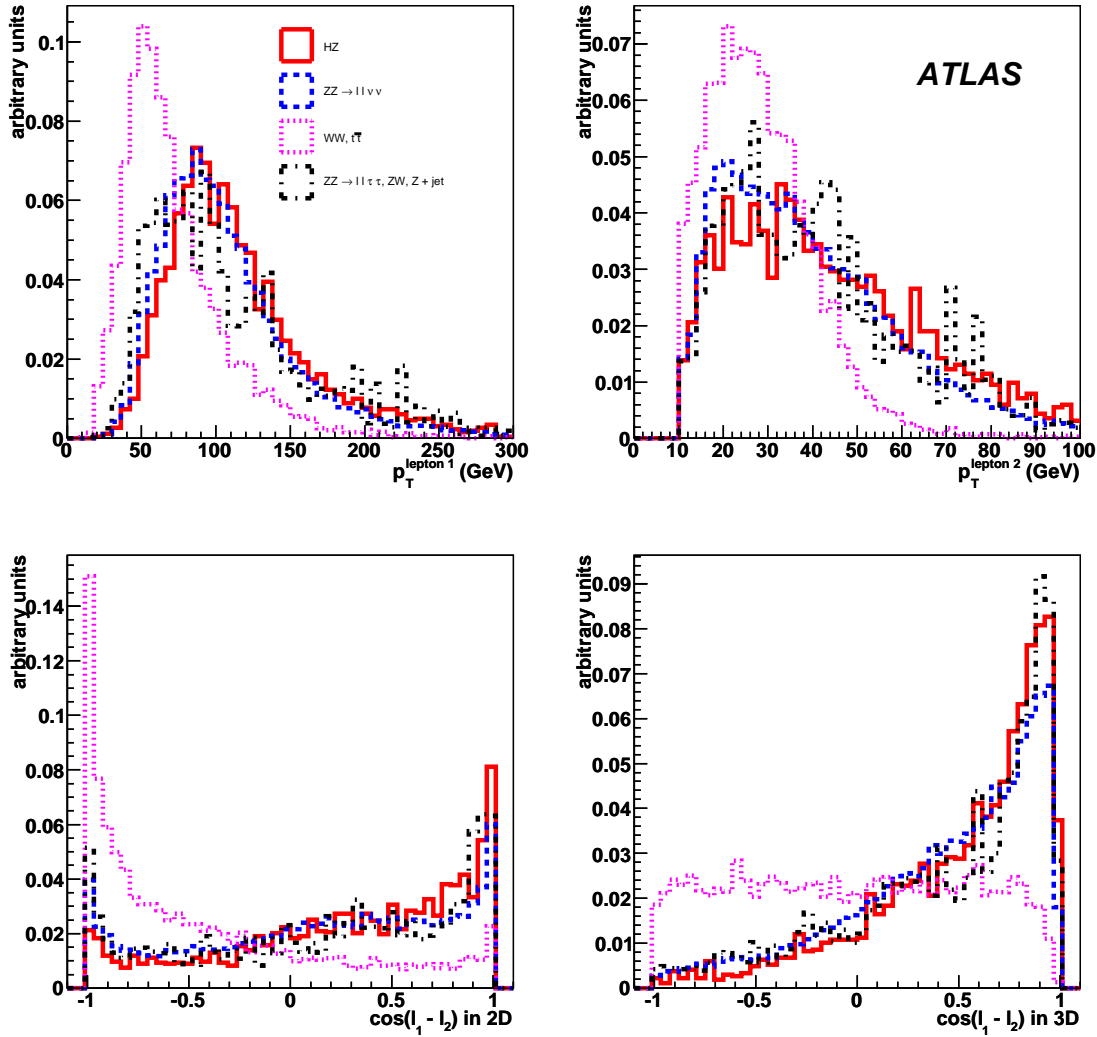
Figure 9: Input variables used by the Boosted Decision Tree for the signal with $m_H = 130$ GeV and the main backgrounds. Top left: Transverse momentum of the most energetic lepton. Top right: Transverse momentum of the second lepton. Bottom left: Cosine of the angle between the two leptons in the transverse plane and, Bottom right: in 3-dimensions. Each plot has been normalized to unity. The combined samples had first been scaled to the same luminosity.
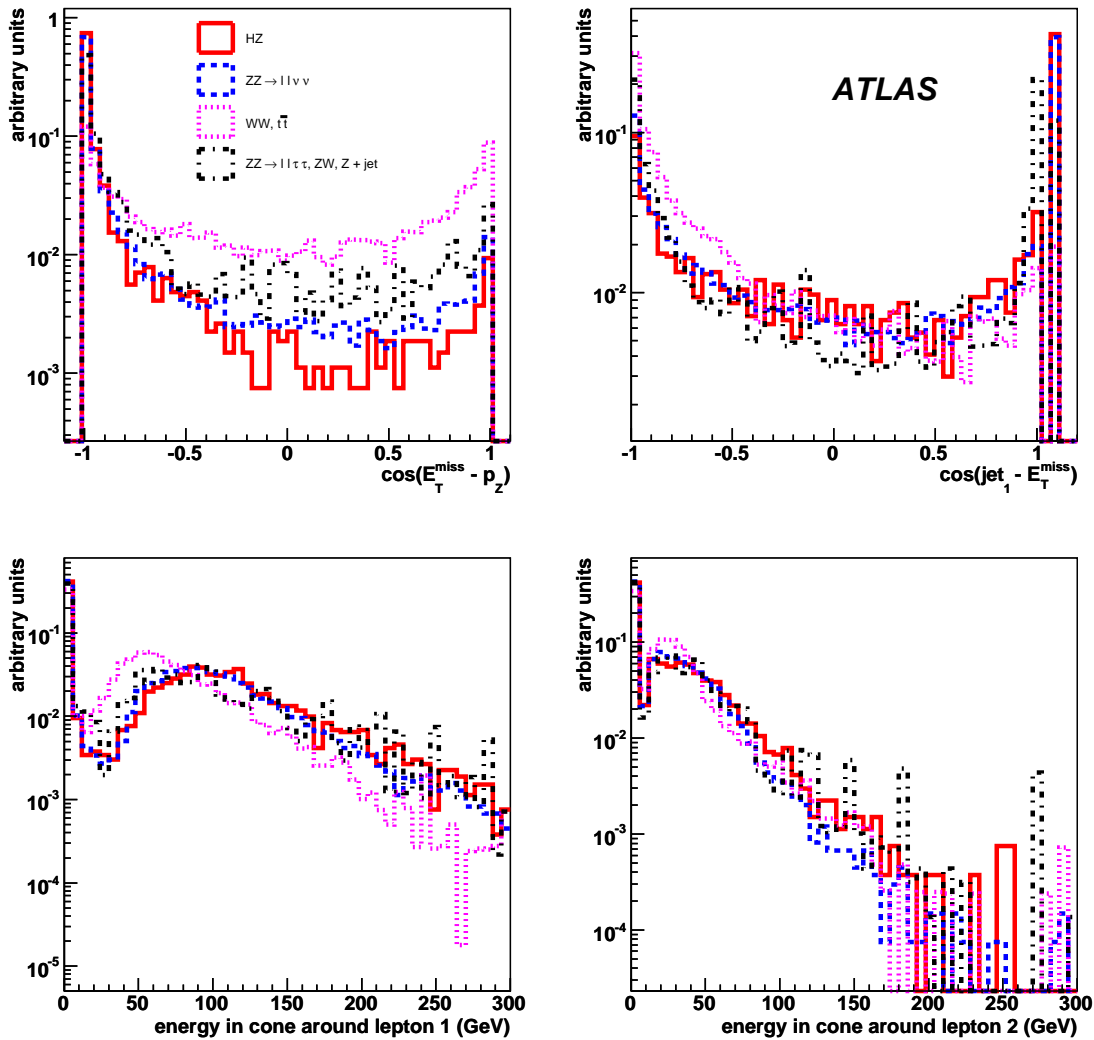
Figure 10: Input variables used by the Boosted Decision Tree for the signal with $m_H = 130$ GeV and the main backgrounds. Top left: The cosine of the angle between the direction of missing E_T and the reconstructed Z transverse momentum. Top right: The cosine of the angle between the most energetic jet and the direction of missing E_T. Bottom left: The energy contained in a cone of 0.10 rad around the most energetic lepton. Bottom right: The energy contained in a cone of 0.10 rad around the second lepton. Each plot has been normalized to unity. The combined samples had first been scaled to the same luminosity.

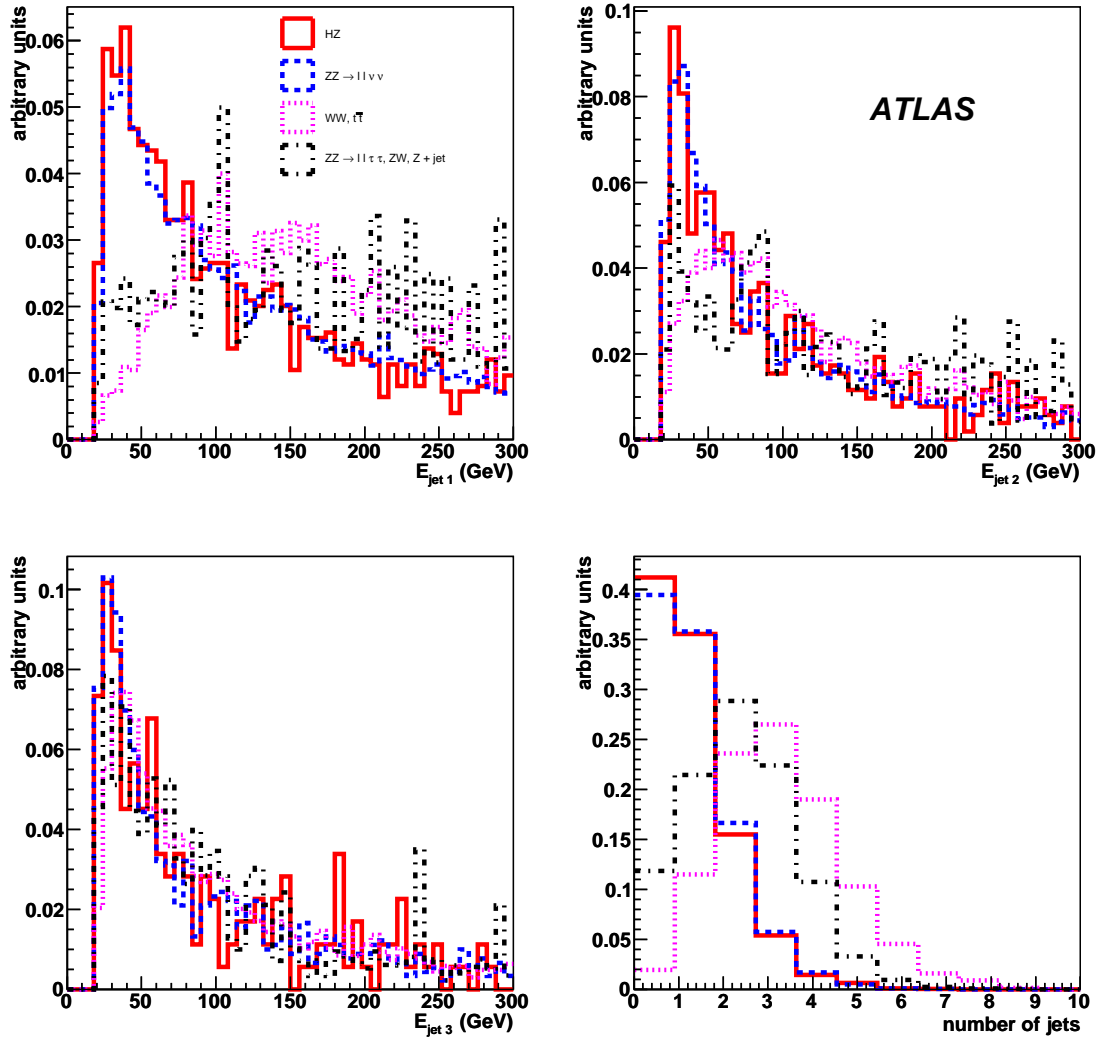Figure 11: Input variables used by the Boosted Decision Tree for the signal with $m_H = 130$ GeV and the main backgrounds. Top left: The energy distribution for the most energetic jet; Top right: for the second and, Bottom left: third most energetic jets. Bottom right: the number of jets in the event. Each plot has been normalized to unity. The combined samples had first been scaled to the same luminosity.
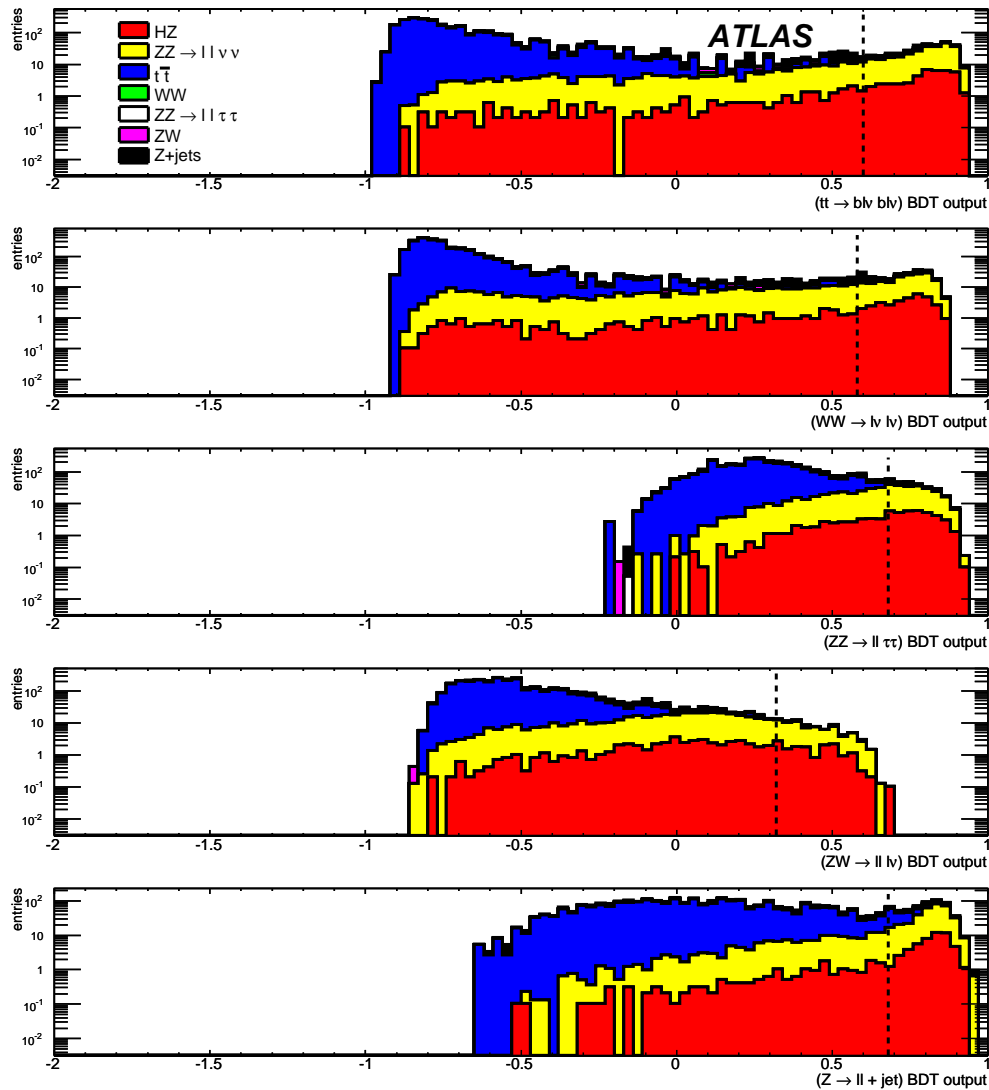
Figure 12: The Boosted Decision Tree (BDT) output variables obtained after comparing half the signal events to five different backgrounds separately, namely, from top to bottom: $t\bar{t} \rightarrow b\ell\nu b\ell\nu$, $WW \rightarrow \ell\nu\ell\nu$, $ZZ \rightarrow \ell\ell\tau\tau$, $ZW \rightarrow \ell\ell\ell\nu$ and $Z \rightarrow \ell\ell + $jets. The BDT assigns values close to +1 for a signal-like event and -1 for background-like events. The distributions are shown for the signal and all types of background when using the other half of the events for the analysis. The Boosted Decision Trees trained against the *ZW* background offers the best separation power. The ξ^2 decreases further once additional cuts on the other BDT output variables are applied, namely the WW BDT output, then the $ZZ \rightarrow \ell\ell\tau\tau$ BDT output, the (Z+jet) BDT output and finally the $t\bar{t}$ BDT output. All BDT output cut values are indicated by a vertical dashed line. Nothing is gained from training a BDT against the irreducible background, $ZZ \rightarrow \ell\ell\nu\nu$ for all Higgs boson mass hypotheses, so it is not used.

input variable to BDT	sum of weights
Z mass	0.57
$\cos \ell\ell$ (in 2D)	0.46
$\cos \ell\ell$ (in 3D)	0.42
$\cos(E_T^{miss} - \vec{p}_Z)$	0.41
# of jets	0.40
transverse mass	0.39
$\cos(jet - E_T^{miss})$	0.32
$\cos E_T^{miss} - p_T^{lepton\#1}$	0.31
E_T^{miss}	0.28
$p_T^{lepton\#1}$	0.27
$E_{jet\#1}$	0.26
$E_{jet\#2}$	0.23
$p_T^{lepton\#2}$	0.21
energy in a cone around lepton # 1	0.17
energy in a cone around lepton # 2	0.16
$E_{jet\#3}$	0.13

Table 10: Order of importance for the 16 input variables used to train the separate Boosted Decision Trees used for the analysis at $m_H = 130$ GeV. The second column gives the sum of the weights given to each input variable by the five separate BDT used for the analysis. These weights are not used for the analysis per se but give an idea of the relative importance of each input variable. In particular, the first four variables are used to mostly reject the non-resonant background.

channel	*ZH* $\ell\bar\ell$ inv.	*ZZ* $\ell\bar\ell\nu\nu$	$t\bar t$	WW $\ell\nu\ell\nu$	*ZZ* $\tau\tau\nu\nu$	*ZZ* $\ell\ell\tau\tau$	ZW $\ell\ell\ell\nu$	Z+jet $\ell\ell$+jet
	expressed as cross-sections given in fb							
$m_H = 110$ GeV	1.31	3.44	0.00	0.01	0.00	0.02	0.37	0.03
$m_H = 120$ GeV	2.99	13.64	0.18	0.28	0.00	0.16	2.16	0.10
$m_H = 130$ GeV	0.89	2.93	0.00	0.00	0.00	0.02	0.33	0.00
$m_H = 140$ GeV	0.98	3.51	0.00	0.00	0.00	0.03	0.48	0.00
$m_H = 150$ GeV	1.32	6.37	0.18	0.00	0.00	0.06	0.62	0.00
$m_H = 200$ GeV	0.62	4.83	0.18	0.00	0.00	0.04	0.42	0.00
$m_H = 250$ GeV	0.31	2.50	0.00	0.00	0.00	0.03	0.24	0.02
	# of events corresponding to 30 fb^{-1}							
$m_H = 110$ GeV	39.2	103.1	<2.7	0.2	<0.01	0.8	11.0	0.8
$m_H = 120$ GeV	89.6	409.3	5.4	8.5	0.1	4.7	64.7	3.0
$m_H = 130$ GeV	26.8	87.9	<2.7	<0.06	<0.01	0.8	9.9	<0.36
$m_H = 140$ GeV	39.5	191.1	5.4	<0.06	<0.01	1.7	18.7	<0.36
$m_H = 150$ GeV	36.5	173.0	5.4	0.2	<0.01	1.8	19.0	<0.36
$m_H = 200$ GeV	18.5	145.0	5.4	<0.06	<0.01	1.3	12.7	<0.36
$m_H = 250$ GeV	9.3	74.9	<2.7	<0.06	<0.01	1.0	7.2	0.7

Table 11: Monte Carlo estimates of the cross-sections in fb surviving the final Boosted Decision Tree selection cuts for each background process and seven mass hypotheses for the ZH channel. The corresponding numbers of events for 30 fb^{-1} of total integrated luminosity are also given. The final cuts on the Boosted Decision Tree output variables were set separately for each BDT output variable and for each mass hypothesis, each time optimizing the sensitivity ξ^2.

3.3 Systematic uncertainties

3.3.1 Background cross-section

Since this is a counting experiment, one is looking for events in excess of what is expected by the Standard Model. However, exactly what is expected from Standard Model backgrounds is not well known, given the theoretical uncertainties on the Standard Model production cross-sections and this leads to the main source of systematic uncertainty. The current best estimates for each of these cross-sections from the next-to-leading order calculation is about 6% for *ZZ* and 5% for *ZW* [21]. The uncertainty on the (Z+jet) cross-section has no impact on the final results since this background is negligible. Several control samples can be used to constrain the ZZ and ZW cross-sections. For *ZZ*, one can use the four lepton final state (even including τ) but this will require a large data sample (of the order of at least 30 fb^{-1}) to reduce the statistical uncertainty. For the ZW cross-section, one can use a ZW control sample with events containing three identified leptons. Both these cross-sections will be measured in ATLAS data. Uncertainties associated with kinematic distributions have not been taken into account at this point. A combined theoretical uncertainty of 5.8% obtained from a weighted average is assigned to the background production cross-section.

One could in principle use $ZZ \to \ell\ell\ell\ell$ events from data to calibrate the number of events coming from $ZZ \to \ell\ell\nu\nu$ decays. Such an approach was proposed in [22] where one would first select a pure sample of $ZZ \to \ell\ell\ell\ell$ events by finding two Z bosons, then declaring one Z to decay invisibly. This would work in the absence of other backgrounds but it is not possible to completely eliminate the $ZW \to \ell\ell\ell\nu$ background. More importantly, such a technique has a very low efficiency: about 1.8% of all $ZZ \to \ell\ell\ell\ell$ survive the preselection cuts, with ℓ here being e, μ or τ. Only a dozen of events would survive all of the BDT selection cuts for 30 fb^{-1} of data. Hence, it is deemed impossible to calibrate quantitatively the $ZZ \to \ell\ell\ell\ell$ cross-section using this technique. However, one could still check the effect of the preselection cuts on $ZZ \to \ell\ell\ell\ell$ events with two leptons declared invisible as described above to ensure that the main and irreducible background, $ZZ \to \ell\ell\nu\nu$, behaves as expected under these cuts. About 85 $ZZ \to \ell\ell\ell\ell$ events are expected to pass the preselection cuts, as opposed to 163 $ZZ \to \ell\ell\nu\nu$ events for 30 fb^{-1} of integrated luminosity. After the preselection cuts, the $ZZ \to \ell\ell\nu\nu$ background corresponds to about 36% of the total number of selected events in the absence of non Standard Model contributions, as seen from Table 8. This method would provide a normalization of the cross-section using data at about 11% uncertainty level.

3.3.2 Effect related to the training of the Boosted Decision Tree

Since half the events are used for training the BDT, and the other half for testing, this arbitrary choice has a slight effect on the outcome. For the central value of this analysis, we used every other event for the training. To estimate the effect of this choice, the analysis was redone using the first half of the events for training, and the second half for testing. Since we are only using Monte Carlo events, this second choice does not introduce additional time-dependent effects that one would expect with real data. The difference in the results, namely +0.2% signal events and +0.7% background events, is ascribed as a contribution to the systematic uncertainty.

3.3.3 Lepton momentum resolution effect and energy scale effect

Different tests are done to assess the contributions to the systematic uncertainty from the lepton momentum resolution and the uncertainty on the lepton energy scale. Each time, new modified input variables are used to retrain the BDT and assess the overall effect by comparing the new number of selected signal and background events to the original numbers of events selected. All contributions to the systematic uncertainty are summarized in Table 12.

	signal	background
electron reconstruction efficiency	$\pm0.2\%$	$\pm0.2\%$
electron p_T resolution ($\pm0.73\%$)	$+0.5\%$	$+1.7\%$
electron energy scale ($\pm0.5\%$)	$+1.1\%$	$+2.1\%$
sub-total for electrons (43% of events)	$+1.2\%$ -0.2%	$+2.7\%$ $- 0.2\%$
muon reconstruction efficiency	$\pm1.0\%$	$\pm1.0\%$
muon p_T resolution (see formula in text)	$+1.1\%$	$+1.9\%$
muon energy scale ($\pm1\%$)	$+1.0\%$	$+2.2\%$
sub-total for muons (57% of events)	$+1.8\%$ $- 1.0\%$	$+3.1\%$ $- 1.0\%$
combined contributions for leptons	$+1.5\%$ $- 0.7\%$	$+2.9\%$ $- 0.7\%$
jet energy scale ($\pm7\%$ or $\pm15\%$)	$+0.8\%$	$+0.2\%$ $- 2.2\%$
jet energy resolution effect on E_T^{miss}	-2.2%	-0.4%
luminosity	-	$\pm3.0\%$
cross-section	-	$\pm5.8\%$
filter effects	$\pm1.4\%$	$\pm1.4\%$
Boosted Decision Tree training effects	$\pm0.2\%$	$\pm0.7\%$
total	$+2.2\%$ $- 2.6$ %	$+7.3\%$ $- 7.1\%$

Table 12: Contributions to the systematic uncertainties. The Higgs boson mass was set to 130 GeV to assess these uncertainties. The final background uncertainty is rounded-off to $\pm7.2\%$.

The tests performed are:

- The lepton momenta are smeared using a Gaussian distribution. A constant sigma of 0.73% is used for electrons. For muons, the sigma is calculated using the following formula: $\sigma(p_T) = [(0.011 \cdot p_T)^2 + (0.00017 \cdot p_T^2)^2]^{1/2}/p_T$ with p_T in GeV. The smearing is applied to one type of leptons at a time.

- For each type of lepton, a multiplicative scaling factor is applied to simulate an energy scale uncertainty of $\pm0.5\%$ for electrons and $\pm1.0\%$ for muons.

3.3.4 Jet momentum resolution effect and energy scale effect

Three different modifications are done in turn to the jet energy to evaluate the contributions from the jet energy scale and jet energy resolution to the missing energy evaluation. After each modification, the missing E_T is recalculatedEach contribution is shown in Table 12. The three modifications made to the jet energy are:

- Jet energy scale: the jet energy is increased by $\pm7\%$ for jets within $\eta \leq 3.2$ and $\pm15\%$ for jets within $\eta > 3.2$.

- Jet energy resolution: the jet energy is smeared using a Gaussian by $0.45 \cdot \sqrt{E}$ for jets within $\eta \leq 3.2$ and $0.63 \cdot \sqrt{E}$ for $\eta > 3.2$.

3.4 Results for the ZH channel

The sensitivity with 30 fb^{-1} of data is evaluated in terms of ξ^2 with $\xi^2 = 1.64\sigma_B/N_S$ for a 95% CL as for the VBF analysis where σ_B is the combined statistical and systematic uncertainty as detailed in Section 2.5. The values of ξ^2 are summarized in Table 13.

m_H	# signal	# background	σ_B	ξ^2
110 GeV	39.2	115.9	13.6	56.7%
120 GeV	82.5	449.4	38.3	76.2%
130 GeV	26.8	98.6	12.2	74.4%
140 GeV	39.5	217.0	21.3	88.5%
150 GeV	36.5	199.4	20.0	89.9%
200 GeV	18.5	164.4	17.3	153.4%
250 GeV	9.3	83.8	10.9	191.6%

Table 13: The sensitivity with 30 fb^{-1} at 95% confidence level calculated in terms of ξ^2 for seven different mass hypotheses for the ZH channel.

3.5   Cross-checks with a cut-based analysis

To ensure that the Boosted Decision Tree performed as expected, we used the same cuts as used in a previous ATLAS analysis performed using a simple cuts approach [22]. The same cuts as in Ref. [22] were applied to our current Monte Carlo samples after the filter and trigger cuts of this analysis, and using the signal generated with $m_H = 130$ GeV. The cuts applied are:

1. Filter cuts as in this analysis

2. Trigger cuts as in this analysis

3. Lepton cuts: select events containing no more than two leptons with $p_T > 7$ GeV. Electrons must have $p_T > 15$ GeV within $|\eta| < 2.5$ and muons are selected if $p_T > 10$ GeV and $|\eta| < 2.4$. Two leptons of the same flavor but opposite charge are required.

4. Z mass: the recontructed Z mass must be within 10 GeV from the pole mass.

5. $E_T^{miss} > 100$ GeV.

6. Jet veto: all events containing a jet having $p_T > 30$ GeV within $|\eta| < 4.9$ are rejected.

7. b-jet veto: all events containing a b-tagged jet having at $p_T > 15$ GeV within $|\eta| < 4.9$ are rejected.

8. Transverse mass: $m_T > 200$ GeV.

The two analyses can be compared after the MET cut. The sensitivity with 30 fb^{-1} at 95% confidence level calculated in terms of ξ^2 for this cut-based analysis is 87.9% for $m_H = 130$ GeV. This compares well with what was obtained with the BDT technique ($\xi^2 = 74.4\%$ for the same mass value with the BDT approach). The difference in sensitivity increases further for higher Higgs mass hypotheses. The results are given in Table 14.

4   Comparison of results and summary

The sensitivity of ATLAS to an invisibly decaying Higgs boson produced via the VBF and *ZH* channel has been examined. A comparison between the sensitivities of the two channels can be seen in Figure 13. This plot shows that the channels have a similar sensitivity for low Higgs boson masses. It is possible to look at combined statistics for the ZH analysis and the VBF shape analyses although the analysis techniques are different. Clearly the improvement in sensitivity by combining statistics is not large. Of

channel	ZH $\ell\bar{\ell}$ inv.	ZZ $\ell\bar{\ell}\nu\nu$	$t\bar{t}$	WW $\ell\nu\ell\nu$	ZZ $\tau\tau\nu\nu$	ZZ $\ell\ell\tau\tau$	ZW $\ell\ell\ell\nu$	Z+jet $\ell\ell$+jet
σ*BR in fb	46.2	728.0	833000.0	5245.6	364.0	123.0	820.0	3105062.8
after filter	34.9	212.6	9412.9	236.5	18.8	87.8	820.0	478.4
after trigger	32.5	198.5	8620.6	217.1	14.2	77.8	735.3	460.6
p_T lepton +ID + charge cut	23.8	148.1	4451.2	158.4	2.7	37.6	177.5	221.6
after $m_Z \pm 10$ GeV cut	20.7	133.0	1654.7	51.1	0.0	28.8	125.4	192.9
after $E_T^{miss} > 100$ cut	7.4	44.9	460.7	7.3	0.0	0.8	13.7	27.9
no jet with $p_T > 30$ GeV	4.2	23.7	5.8	0.8	0.0	0.3	4.2	0.1
b-tag cut for jet with $p_T > 15$ GeV	4.2	23.6	4.8	0.8	0.0	0.3	4.1	0.1
after $m_T > 200$ GeV cut	3.9	21.3	0.5	0.4	0.0	0.3	3.4	0.1

Table 14: Monte Carlo estimates of the cross-sections in fb after applying simple cuts for each background process and one mass hypothesis of $m_H = 130$ GeV for the ZH channel. The corresponding ξ^2 would be 87.9%.

far greater significance in the analysis of real ATLAS data would be the observation of a significant excess of events in two different and distinct channels. An observation of this kind would give credibility to the hypothesis that a particle is being generated that behaves like a Higgs boson and decays invisibly.

In summary, a study using fully simulated ATLAS data has shown that the ATLAS experiment will be sensitive to an invisibly decaying Higgs boson in both the VBF and *ZH* production channels assuming only Standard Model backgrounds. It is clear that the analysis will require a good understanding of the experimental systematic uncertainties. If the decay of a Higgs boson was entirely in the invisible mode, this analysis has shown that with 30 fb^{-1}of data, ATLAS will be sensitive to a situation in which the beyond the Standard Model cross-section is of the order of 80% the Standard Model Higgs boson cross-sections for a Higgs Boson mass of less than 150 GeV. The VBF analysis has a sensitivity of better than 90% up to a Higgs Boson mass of 250 GeV.

References

[1] K. Greist, H. E. Haber, Phys. Rev. **D37** (1988) 719; A. Djouadi, J. Kalinowski, P. M. Zerwas, Z. Phys. **C57** (1993) 569; A. Djouadi, P. Janot, J. Kalinowski, P. M. Zerwas, Phys. Lett. **B376**(1996) 220; I. Antoniadis, M. Tuckmantel, F. Zwirner, Nucl. Phys. **B707** (2005) 215.

[2] J. C. Romao, F. de Campos, J. W. F. Valle, Phys. Lett. **B292** (1992) 329; M. Hirsch, J. C. Romao, J. W. F. Valle; A. V. Moral, *Invisible Higgs Boson Decays in Spontaneously Broken R-Parity,* hep-ph/0407269.

[3] N. Arkani-Hamed, S. Dimopoulos, G. Dvali, J. March-Russell, Phys. Rev. **D024032** (2002) 1264; A. Datta, K. Huitu, J. Laamanen, B. Mukhopadhyaya, Phys. Rev. **D70** (2004) 075003; K. M. Belotsky, V. A. Khoze, A. D. Martin, M. G. Ryskin, Eur. Phys. J. **C36** (2004) 503; D. Dominici, hep-ph/0408087 (2004); J. Laamanen, hep-ph/0505104 (2005); D. Dominici, hep-ph/0503216 (2005); M. Battaglia, D. Dominici, J. F. Gunion, J. D. Wells, hep-ph/0402062 (2004); A. Datta, K. Huitu, J. Laamanen, B. Mukhopadhyaya, Phys. Rev. **D70** (2004) 075003.

[4] LEP Higgs Working Group, *Searches for invisible Higgs bosons: Preliminary combined results using LEP data collected at energies up to 209 GeV*, hep-ex/0107032 (2001).
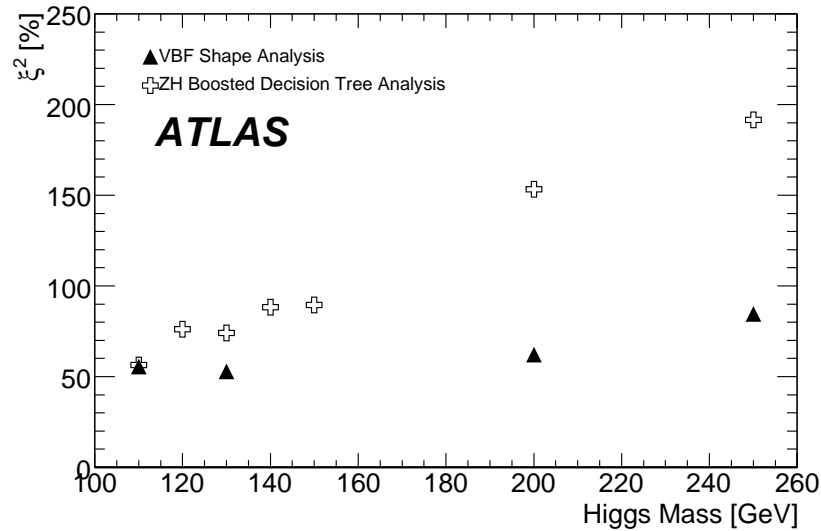
Figure 13: Sensitivity to an invisible Higgs boson with ATLAS for both the VBF and *ZH* channels with 30 fb^{-1}of data assuming only Standard Model backgrounds. The open crosses show the sensitivity for the *ZH* analysis and the solid triangles show the sensitivity for the VBF shape analysis for 95 % CL. Both these results include systematic uncertainties.

[5] O. J. P. Éboli, D. Zeppenfeld,, Phys. Lett. B **495** (2000) 147.

[6] J. F. Gunion, Phys. Rev. Lett. **72** (1994) 199.

[7] D. Choudhury, D. P. Roy, Phys. Lett. B **232** (1994) 368.

[8] R. M. Godbole, M. Guchait, K. Mazumdar, S. Moretti, D.P. Roy, Phys. Lett. B **1571** (2003) 1284.

[9] ATLAS Collaboration, *Introduction on Higgs Boson Searches at the Large Hadron Collider*, this volume.

[10] P. Gagnon, *Invisible Higgs boson decays in the ZH and WH channels*, ATL-PHYS-PUB-2005-011 (2005).

[11] G. Corcella et al., *Herwig 6.5 Release Note*, hep-ph/0210213v2 (2005).

[12] J. M. Butterworth, J. R. Forshaw, M. H. Seymour, Z. Phys. **C72** (1996) 637–646.

[13] J. M. Butterworth, M. H. Seymour, *Jimmy4: Multiparton Interactions in Herwig for the LHC*, http://projects.hepforge.org/jimmy/draft20051116.ps.

[14] T. Sjostrand, S. Mrenna, P. Skands, *PYTHIA 6.4 Physics and Manual*, hep-ph/0603175 (2006).

[15] B. Mellado, A. Nisati, D. Rebuzzi, S. Rosati, G. Unal, S. L. Wu, *Higgs Production Cross-Sections and Branching Ratios for the ATLAS Higgs Working Group*, ATL-COM-PHYS-2007-024 (2007).

[16] ATLAS Collaboration, *Monte Carlo Production*, this volume.

[17] M. L. Mangano, M. Moretti, F. Piccinini, R. Pittau, A. Polosa, JHEP **07** (2003) 001.

[18] ATLAS Collaboration, *Jet and Missing Et Combined Performance CSC Chapter*, this volume; AT-LAS Collaboration, *b-Tagging CSC Chapter*, this volume; ATLAS Collaboration, *Electron/Photon CSC Chapter*, this volume; ATLAS Collaboration, *Muon CSC Chapter*, this volume.

[19] ATLAS Collaboration, *Cross-sections for Standard Model processes to be used in the ATLAS CSC notes*, this volume.

[20] A. Höcker et al., *TMVA - Toolkit for Multivariate Data Analysis,* CERN-OPEN-2007-007, ACAT 040, 2007, arXiv: physics/0703039, http://tmva.sf.net/.

[21] ATLAS Collaboration, *Diboson Physics Studies With the ATLAS Detector*, this volume.

[22] F. Meisel, M. Duhrssen, M. Heldmann, K. Jakobs, *Study of the discovery potential for an invisibly decaying Higgs boson via the associated ZH production in the ATLAS experiment*, ATL-PHYS-PUB-2006-009 (2006).